

Stellar population properties for 2 million galaxies from SDSS DR14 and DEEP2 DR4 from full spectral fitting

Johan Comparat¹, Claudia Maraston², Daniel Goddard², Violeta Gonzalez-Perez^{2,10}, Jianhui Lian², Sofia Meneses-Goytia^{2,11}, Daniel Thomas², Joel R. Brownstein³, Rita Tojeiro⁴, Alexis Finoguenov^{1,9}, Andrea Merloni¹, Francisco Prada⁵, Mara Salvato¹, Guangtun B. Zhu⁶, Hu Zou⁷, and Jonathan Brinkmann⁸

¹ Max-Planck-Institut für extraterrestrische Physik (MPE), Giessenbachstrasse 1, D-85748 Garching bei München, Germany
e-mail: comparat@mpe.mpg.de

² Institute of Cosmology and Gravitation, University of Portsmouth, Portsmouth, PO1 3FX, UK

³ Department of Physics and Astronomy, University of Utah, 115 S. 1400 E., Salt Lake City, UT 84112, USA

⁴ School of Physics and Astronomy, North Haugh, St. Andrews KY16 9SS, UK

⁵ Instituto de Astrofísica de Andalucía (CSIC), Glorieta de la Astronomía, E-18080 Granada, Spain

⁶ Center for Astrophysical Sciences, Department of Physics and Astronomy, Johns Hopkins University, 3400 North Charles Street, Baltimore, MD 21218, USA

⁷ Key Laboratory of Optical Astronomy, National Astronomical Observatories, Chinese Academy of Sciences, Beijing 100012, China

⁸ Apache Point Observatory, P.O. Box 59, Sunspot, NM 88349

⁹ Department of Physics, University of Helsinki, Gustaf Hällströmin katu 2a, FI-00014 Helsinki, Finland

¹⁰ Energy Lancaster, Lancaster University, Lancaster LA14YB, UK

¹¹ Department of Physics, University of Surrey, Guildford GU2 7XH, UK

Received Nov 16, 2017

ABSTRACT

Aims. We determine the stellar population properties - age, metallicity, dust reddening, stellar mass and the star formation history - for all spectra classified as galaxies that were published by the Sloan Digital Sky Survey (SDSS data release 14) and by the DEEP2 (data release 4) galaxy surveys.

Methods. We perform full spectral fitting on individual spectra, making use of high spectral resolution stellar population models. Calculations are carried out for several choices of the model input, including three stellar initial mass functions and three input stellar libraries to the models. We study the accuracy of parameter derivation, in particular the stellar mass, as a function of the signal-to-noise of the galaxy spectra. We find that at low redshift, a signal to noise ratio per pixel around 20 (5) allows a statistical accuracy on $\log_{10}(M^*/M_{\odot})$ of 0.2 (0.4) dex, for the Chabrier IMF.

Results. For the first time, we study DEEP2 galaxies selected by their [OIII] luminosity in the redshift range $0.83 < z < 1.03$, finding that they are consistent with a flat number density in stellar mass in the range $10^9 < M/M_{\odot} < 10^{11.5}$. We find the resulting stellar mass function based on SDSS or eBOSS in agreement with previous studies (e.g. Maraston et al. 2013). We publish all catalogs of properties as well as model spectra of the continuum for these galaxies as a value added catalog of the fourteenth data release of the SDSS. This catalog is about twice as large as its predecessors (DR12) and will aid a variety of studies on galaxy evolution and cosmology.

Key words. galaxy evolution - stellar population model - galaxy surveys

Contents

1	Introduction	3
2	Spectroscopic data	3
2.1	SDSS	3
2.2	DEEP2	4
3	Obtaining the stellar population properties of galaxies	4
3.1	The Firefly fitting routine	4
3.2	Maraston & Strömbäck (2011) models	5
3.3	Input parameters	5
4	Resulting galaxy parameters	10
4.1	Ages and metallicities	10
4.2	Dust and stellar masses	10
4.3	Star Formation history	12
5	Results	15
5.1	SDSS and eBOSS	15
5.2	DEEP2	15
5.3	General findings as a function of parameters.	16
5.4	Ages, metallicities and star formation histories of galaxies	21
6	Applications	24
6.1	Stellar mass function of galaxies selected with their [OIII] emission line luminosity in DEEP2	24
6.2	Stellar mass function probed by SDSS, eBOSS and DEEP2	24
7	Summary and future releases	26
8	Acknowledgements	26
A	Description of the FIREFLY data	28
A.1	Processing	28
A.2	Public FIREFLY catalogs and data	28
B	Warning about fits with unconstrained parameters	29
C	Large tables	29

1. Introduction

In the current paradigm of galaxy evolution, structures and galaxies form hierarchically: larger halos are formed by the coalescence of smaller progenitors. From a macroscopic or thermodynamical point of view, galaxies are typically described as systems composed by tightly interacting sub-systems: a dark matter halo, a central black hole, stars, cold gas, hot gas and dust. The visible component of galaxies is approximated as a tri-phased system made of stars, inter-stellar medium and circum-galactic medium. A galactic system is governed by various processes, such as star formation rate, supernovae rate, the active galactic nuclei which - when present - is held to regulate gas dynamics, such as winds, accretion and outflows (Mo et al. 2010). The composition of stellar populations in galaxies is thus a key aspect of galaxy formation and evolution.

The classical method to infer the stellar properties of galaxies (e.g. stellar ages, chemical composition, dust, the star formation history and the stellar mass) is to fit stellar population model spectra to the observed spectral energy distribution. Several input physics and parameters enter this approach and determine the resulting galaxy properties, namely: the stellar population model and its input physics (i.e. stellar evolution and atmosphere models); the wavelength range spanned by observations and models; the fitting method to compare models and data (e.g. statistics, priors, etc.). In this study we use the Maraston & Strömbäck (2011) (M11 hereafter) stellar population models together with the FIREFLY fitting routine (hereafter FF Wilkinson et al. 2015; Goddard et al. 2017a,b; Wilkinson et al. 2017). These code and models have been shown to be able to accurately reconstruct a galaxy star formation history from spectra with signal to noise ratios (SNR) of about 5 per pixel (see, Wilkinson et al. 2017, and Sec. 3.1). FF was used in the following recent stellar population studies using SDSS-IV MANGA integral field spectroscopy data: Wilkinson et al. (2015); Goddard et al. (2017a,b); Lian et al. (2018a,b); Parikh et al. (2018).

We perform model fitting to the optical spectra measured by the Sloan Digital Sky Survey (SDSS DR14 Abolfathi et al. 2017) and the DEEP2 survey (DR4 Newman et al. 2013). We chose these two medium resolution optical spectroscopic surveys because they sample the observed magnitude vs. redshift plane in a complementary manner. Stellar population model catalogs are available for the SDSS DR12. These consist of stellar properties obtained from broad-band SED fitting (Maraston et al. 2013) and emission-line properties by Thomas et al. (2013). In this work we extend those approaches by employing full spectral fitting and we extend the calculations to a substantially larger data set.

The paper is organised as follows. The adopted set of observed spectra are presented in Section 2. The FIREFLY fitting routine and the stellar population models are described in Section 3. We present the results obtained for the four main fitted parameters - namely stellar ages, chemical composition, dust reddening and stellar mass - in Section 4 and in Section 5, we discuss the global results obtained for each set of observed spectra. Finally in Section 6.1, we calculate for the first time the stellar mass function of [OII] emitters in DEEP2 and discuss the scientific implications of our findings.

Throughout the work we assume a standard flat Λ CDM (Planck Collaboration et al. 2014) cosmology. The software is available at the official FIREFLY page¹ and through GitHub². The results are available through the FIREFLY data repository³.

2. Spectroscopic data

In this analysis, we consider galaxy spectra taken from both the SDSS and DEEP2 spectroscopic surveys. The redshift range spanned by the data is $0 < z < 1.7$. As we shall see most derived stellar masses are in the range $10^6 M_{\odot}$ to $10^{12.5} M_{\odot}$. These two surveys cover the parameter space of galaxy evolution in a complementary fashion. SDSS covers the most luminous galaxies over a wide area (order of $10,000 \text{ deg}^2$) and DEEP2 samples fainter galaxies (by about 2 magnitudes, over a much smaller area (order of 2 deg^2). More details are provided in the next subsections.

2.1. SDSS

We consider galaxy spectra obtained with either the SDSS or BOSS spectrograph (Gunn et al. 2006; Smee et al. 2013) as in the fourteenth data release (Dawson et al. 2016; Blanton et al. 2017; Abolfathi et al. 2017). The SDSS (BOSS) spectrographs cover $3800\text{-}9200\text{\AA}$ ($3650 - 10,400\text{\AA}$) at a resolution 1500 at 3800\AA and 2500 at 9000\AA with 3 (2) arc seconds diameter fibers. Due to the variety of target selection algorithms successively applied to target galaxies within SDSS, the magnitude limit assumes different values. In the *i*-band, the various magnitude limits lie mostly within the range 17 to 22.5. After the twelfth data release of SDSS, the program using the BOSS spectrograph was extended into the extended-BOSS (eBOSS) program. In the following we use eBOSS to designate spectroscopic data acquired with the BOSS spectrograph and released in the DR14.

For the stellar population fitting, we consider objects classified as galaxies following criteria used in previous SDSS galaxy products⁴. We consider objects for which a definite positive redshift was derived using galaxy templates (`CLASS=="GALAXY"`, `Z > ZERR > 0`, `ZWARNING == 0`) in the current redshift pipeline (Bolton et al. 2012, version v5_10_0). For the data obtained with the BOSS spectrograph, we consider the "NOQSO" version of these quantities. We finally retrieve about 2.7 million optical galaxy spectra, of which 948,259 were observed with the SDSS spectrograph setup and with 1,759,362 with the BOSS spectrograph setup. The SDSS (BOSS) spectrograph allows 640 (1000) fibers of 3 (2) arc-seconds diameter per plate to be plugged and covers the wavelength range $3,800\text{-}9,200$ ($3,600\text{-}10,400$) Angstroms with two arms.

¹ <http://www.icg.port.ac.uk/firefly/>

² <https://github.com/FireflySpectra/>

³ https://firefly.mpe.mpg.de/v1_1_0/

⁴ <http://www.sdss.org/dr12/spectro/galaxy/>

Data source

The full set of observed spectra we processed occupies about 0.8T of disk space. This data is available via the SDSS server,

- BOSS spectrograph data
https://dr14.sdss.org/sas/dr14/eboss/spectro/redux/v5_10_0/spectra/PLATE/spec-PLATE-MJD-FIBERID.fits
- SDSS spectrograph data
<https://dr14.sdss.org/sas/dr14/sdss/spectro/redux/26/spectra/PLATE/spec-PLATE-MJD-FIBERID.fits>

The spectra are described here https://data.sdss.org/datamodel/files/BOSS_SPECTRO_REDUX/RUN2D/spectra/PLATE4/spec.html.

2.2. DEEP2

DEEP2 is a deep pencil beam survey that acquired spectra for galaxies brighter than $R < 24.1$ to study the evolution of galaxies. The survey is split in four fields that cover 2.7 deg^2 (Newman et al. 2013). The DEIMOS spectrograph at Keck was used, which covers approximately the wavelength range $6500 - 9300 \text{ \AA}$ at a resolution ~ 6000 (Faber et al. 2003). It accommodates of the order 120 slits per mask. Although DEEP2 is a major galaxy evolution survey and stellar masses for galaxies observed by DEEP2 are mentioned in several publications, there does not seem to be a publicly available catalogue of stellar mass and other galaxy properties (Kassin et al. 2007; Covington et al. 2010; Mostek et al. 2013; Coil et al. 2017). With our work we fill this gap.

In our analysis we consider galaxy spectra classified with a flag $Z_FLG \geq 2$ and whose redshift lies in the range $0.7 < z < 1.2$. This redshift range allows the sampling of the 4000 \AA break which is needed for a robust recovery of stellar ages. Out of the 50,319 entries in the DEEP2 DR4 catalog, our redshift cut selects $\sim 22,873$ unique objects. We further sort the data according to the detection of emission line in the spectrum. All data is detailed in Table 2. Finally, we use flux-calibrated spectra which were published by Comparat et al. (2016).

The spectra used in this analysis were obtained via the DEEP2 server, here: <http://deep.ps.uci.edu/DR4/spectra.html>. The subset of processed flux-calibrated spectra are available here https://firefly.mpe.mpg.de/v1_1_0/DEEP2/spectra.

3. Obtaining the stellar population properties of galaxies

We adopt the fitting code FIREFLY (Wilkinson et al. 2017) described in Sec. 3.1 and the stellar population models of Maraston & Strömbäck (2011), described in Sec. 3.2. We run the fitting procedure with different options for the Initial Mass Function (IMF) and input stellar library (see 3.3). The details of the various runs are described in Sec. A.1. The FIREFLY data-model generated by our analysis is described in Sec. A.2. We discuss the resulting stellar age, stellar metallicity and stellar mass distributions in Sec. 4.

3.1. The Firefly fitting routine

FIREFLY⁵ is a chi-squared minimization fitting code that for a given input observed Spectral Energy Distribution (SED), compares combinations of single-burst stellar population models (SSP), following an iterative best-fitting process controlled by the Bayesian Information Criterion (BIC) until convergence is achieved. An important feature of this code is that no priors - other than the assumed models and model grid - are applied, rather all solutions within a statistical cut are retained with their weight. The weight of each component can be arbitrary and no regularisation is imposed afterwards (as instead in pPXF, Cappellari & Emsellem 2004). Attenuation by dust is accounted for in a novel way, which is fully described in Wilkinson et al. (2017) and summarised below. As dust attenuation has the effect at distorting the intrinsic continuum shape, the attenuation can be deduced after the intrinsic continuum shape is recovered. To this end we first rectify the continuum shape of both observations and models by multiplying them by a function, which is referred to as High-Pass Filter (HPF). This removes the large-scale modes of the spectra, i.e. those with a width larger than $\sim 100 \text{ \AA}$. We then find the stellar population model best-fitting the rectified data. The best-fit model essentially is the one that best matches the spectral absorption features. The comparison between the original (not rectified) observed spectrum and best-fitting model finally gives the attenuation. The flux difference between the two is used to obtain an attenuation array (i.e. flux ratios per wavelength). The returned attenuation array is then matched to known analytical approximations to return an E(B-V) value. Note that this procedure allows for removal of large scale modes of the spectrum associated with dust but also poor flux calibration (see Wilkinson et al. 2015). Finally, FIREFLY provides both light- and mass-weighted stellar population properties (age and metallicity), E(B-V) values and the stellar mass for the best fitting model and its single-burst components. Errors on these properties are obtained by the likelihood of solutions within the statistical cut.

In summary, the fitting routine follows these steps: i) resolution of models and data are matched (by, usually, downgrading the models); ii) emission lines are masked; iii) dust attenuation is determined as described before; iv) the best fitting stellar population model is obtained as a linear combination of single-burst models; v) χ^2 are converted into probabilities and average properties and errors (both mass weighted and light weighted) are calculated. For full details we refer the readers to Wilkinson et al. (2017). The code and the models used to create this dataset are public via the SDSS server:

- Fitting code. The official website of the FIREFLY team is <http://www.icg.port.ac.uk/firefly> links to the up-to-date version of the FIREFLY software.
- Stellar population models: https://svn.sdss.org/public/data/sdss/stellarpopmodels/tags/v1_0_2/

⁵ <http://www.icg.port.ac.uk/firefly>

Note that we output the actual (present) stellar mass, and its fraction locked in stellar remnants (white dwarfs, neutron stars and black holes) or lost via stellar evolution (returned fraction).

Performances of Firefly and reliability of derived galaxy properties.

Wilkinson et al. (2017) have thoroughly investigated the performances of FIREFLY to recover stellar population properties such as age, metallicity, star formation history and stellar mass, as a function of several variables, in particular the SNR, the amount of reddening, the assumed star formation history, the wavelength range spanned by the data, using both mock galaxies with known input properties as well as real Milky Way star clusters with ages and metallicity determined independently (i.e. via CMD fitting for ages and resolved spectroscopy for metallicity, see Wilkinson et al. 2017 for full details). Here we summarise those findings and refer to the paper for full details and plots.

Firefly is able to recover the stellar population properties (age, metallicity, star formation history and stellar mass) down to a $\text{SNR} \sim 5$, for moderately dusty systems ($E(B-V) < 0.75$) (see Figures 8-16 in Wilkinson et al. 2017). At $\text{SNR} \sim 20$, the recovery of the star formation history is remarkably good independently of reddening, unless the star formation is very extended (~ 10 Gyr). Even at lower SNR down to $\text{SNR} \sim 0.5$, stellar masses are well recovered (e.g. Figure 14) in some cases due to compensating errors in the derived age and metallicity. Spectral stellar masses are in agreement (within errors) with estimates based on SED fitting on broad band magnitudes. Indeed, Wilkinson et al. (2017) compared the FIREFLY-SDSS determinations to the results from Cid Fernandes et al. (2005); Tojeiro et al. (2009) (section 6.2, Figs. 24, 25) for galaxies from the SDSS-II.

Not surprisingly, the age-metallicity-dust degeneracy is more severe in very dusty systems (e.g. Figure 13) or where the age/metallicity degeneracy peaks (e.g. when the red giant Branch becomes an important contributor, hence around 1 Gyr). These degeneracies make individual stellar ages and stellar metallicities less well determined (e.g. Figure 12).

Regarding the effect of the wavelength range spanned by the fitted data, Wilkinson et al. (2017) demonstrated via mock experiments as well as fitting of star clusters with known ages from CMD fitting (section 5.2, Fig. 19) the well-known fact that the 4000Å-break spectral region is needed in order to reliably constrain stellar ages. While SDSS+eBOSS spectra all contain this region, this is not the case for the entire DEEP2 database, in particular for DEEP2 galaxy spectra only covering the wavelength range 6500-9300Å. This implies that accurate ages for DEEP2 galaxies can only be recovered if the redshift is in the window $3800(1+z) > 6500$ and $4200(1+z) < 9300$ i.e. $0.7 < z < 1.2$.

In both cases, a qualitative agreement was found and residual discrepancies were attributed to the priors set in those other codes. Overall we conclude that Firefly is an excellent tool to try and recover galaxy properties in regimes of low S/N.

3.2. Maraston & Strömbäck (2011) models

We use the Maraston & Strömbäck (2011) stellar population models, which are offered for a variety of input stellar libraries at the same energetics. In particular, we shall use M11 models including the following three main libraries:

- STELIB, covers 3200–9300Å with a 3.4Å sampling at 5500Å, i.e. at a resolution $R = 1617$, with 85 eigenvectors (Le Borgne et al. 2003),
- MILES, covers 3500–7430Å with a 2.54Å sampling at 5500Å, i.e. at a resolution $R = 2165$, with 156 eigenvectors (Sánchez-Blázquez et al. 2006; Falcón-Barroso et al. 2011; Beifiori et al. 2011),
- ELODIE, covers 3900–6800Å with a 0.55Å sampling at 5500Å, i.e. at a resolution $R = 10000$, with 132 eigenvectors (Prugniel et al. 2007).

The wavelength range spanned by the models define the redshift range where the model fitting is possible given the wavelength ranges spanned by the data. Recall that the instruments on SDSS, BOSS and DEIMOS cover the ranges 3800 – 9200Å, 3650 – 10,400Å, and 6500 – 9300Å at $R \sim 2000, 2000, 6000$, respectively. The mismatch between the wavelength coverage of DEEP2 and the models explain the lack of fits at low redshift. It is part of an ongoing effort to complete the low-redshift extension of DEEP2 with near-IR extended models, which we shall release in the future.

The reason for performing such a large variety of spectral modelling without choosing one single model rendition is manifold. First of all, it is currently unclear which one of these Milky Way-based empirical libraries is more correct, where correctness means that when implemented in population models, the models are able to recover age and metallicity of known stellar systems. Maraston & Strömbäck (2011) noted that M11-STEELIB models were recovering most accurately the turnoff age of the solar-metallicity Milky Way star cluster W3. On the other hand, STELIB has a limited coverage in sub-solar metallicity, implying that STELIB-based models cannot be fit to metal-poor Milky Way globular clusters, for which MILES-based models were giving a good fit (Maraston & Strömbäck 2011; Wilkinson et al. 2017). Moreover, galaxy evolution studies in the literature are based on models with different input libraries, hence a proper comparison of studies based on the latest SDSS data releases with those early works requires the availability of a variety of models. Indeed, while early SDSS-based galaxy evolution studies were based on STELIB-type models (by Bruzual & Charlot 2003, as e.g. in Kauffmann et al. 2003 or Tremonti et al. 2004), the data analysis of SDSS-IV/MaNGA is mostly based on MILES-type models (by M11, Vazdekis et al. 2016 or Conroy et al. 2014). In addition, we explore the ELODIE-based models which have not been used much in the literature, but allows a higher spectral resolution.

3.3. Input parameters

We perform spectral model fitting for each input M11 model described above (namely, M11-ELODIE, M11-MILES and M11-STEELIB), and for three choices of the stellar initial mass function (IMF), namely Salpeter, Salpeter (1955), Chabrier, Chabrier

(2003) and Kroupa, Kroupa (2001), for each of these models. Hence, in total we provide up to nine modelling of the continuum for each galaxy (depending on whether the parameter 'stellar mass' results to be constrained).

The models span ages in the range $10^6 < \text{Age}[\text{yr}] < 2 \times 10^{10}$ and metallicities in the range $-3 < \log_{10}(Z/Z_{\odot}) < 3$, with each M11 model spanning a different age/metallicity grid (cf. Wilkinson et al. 2017, Table1). Recalling, the total number of ages available for each model flavour are: 85 for M11-STELIB, 132 for M11-ELODIE and 156 for M11-MILES.

The E(B-V) parameter boundaries are 0-0.7.

Examples of spectral fitting results for a SDSS, an eBOSS and a DEEP2 galaxy spectrum are given in Figures 1, 2, 3, where we show the observed spectrum, the fitted models, the distribution of residuals and the main parameters derived. As the assumed IMF has little influence on the spectral modelling, mostly resulting in well-known offsets in the derived stellar mass (e.g. Pforr et al. 2012), for clarity we show the results for one IMF and the three model libraries.

Fig. 1. Example of a fit for a galaxy spectrum randomly taken from a SDSS plate, namely plate=0266, mjd=51602, fiberid=4. This galaxy lies at redshift 0.127. It has a S/N around the 4000Å break of 10.75. The **top panel** shows the observed spectrum (grey line) and its modelling (coloured lines). Each model fit is characterized by the number of SSPs given in the caption. Gaps in the spectrum correspond to regions masked due to the presence of emission lines. The **second panel** shows the χ^2 distribution per pixel for each model compared to a normal distribution (labeled $\mathcal{N}(0,1)$, dashed line). The **third and fourth rows** of panels show the derived galaxy parameters and their 1σ uncertainties. On the **third row** from left to right: mass-weighted age vs. mass-weighted metallicity (Panel 1), mass-weighted age vs. stellar mass (Panel 2) and SSP weights vs. mass-weighted age of the individual SSP components (Panel 3). On the **fourth row** from left to right: Panel 1 shows mass vs. mass-weighted metallicity, Panel 2 shows mass vs. reddening and Panel 3 shows the SSP weights vs. mass-weighted metallicities of the individual SSP components. Results consistently point towards a super-solar mass-weighted metallicity of $10^{0.2}Z_{\odot}$, an old mass-weighted age of 10^{10} yr, an E(B-V) between 0.15 and 0.2, and a stellar mass about $10^{10.75} - 10^{11}M_{\odot}$. STELIB-based models give the most massive and older solution than MILES and ELODIE. The decomposition in SSPs shows the solution is constituted of two old bursts, one with solar metallicity and one with higher metallicity in comparable proportions.

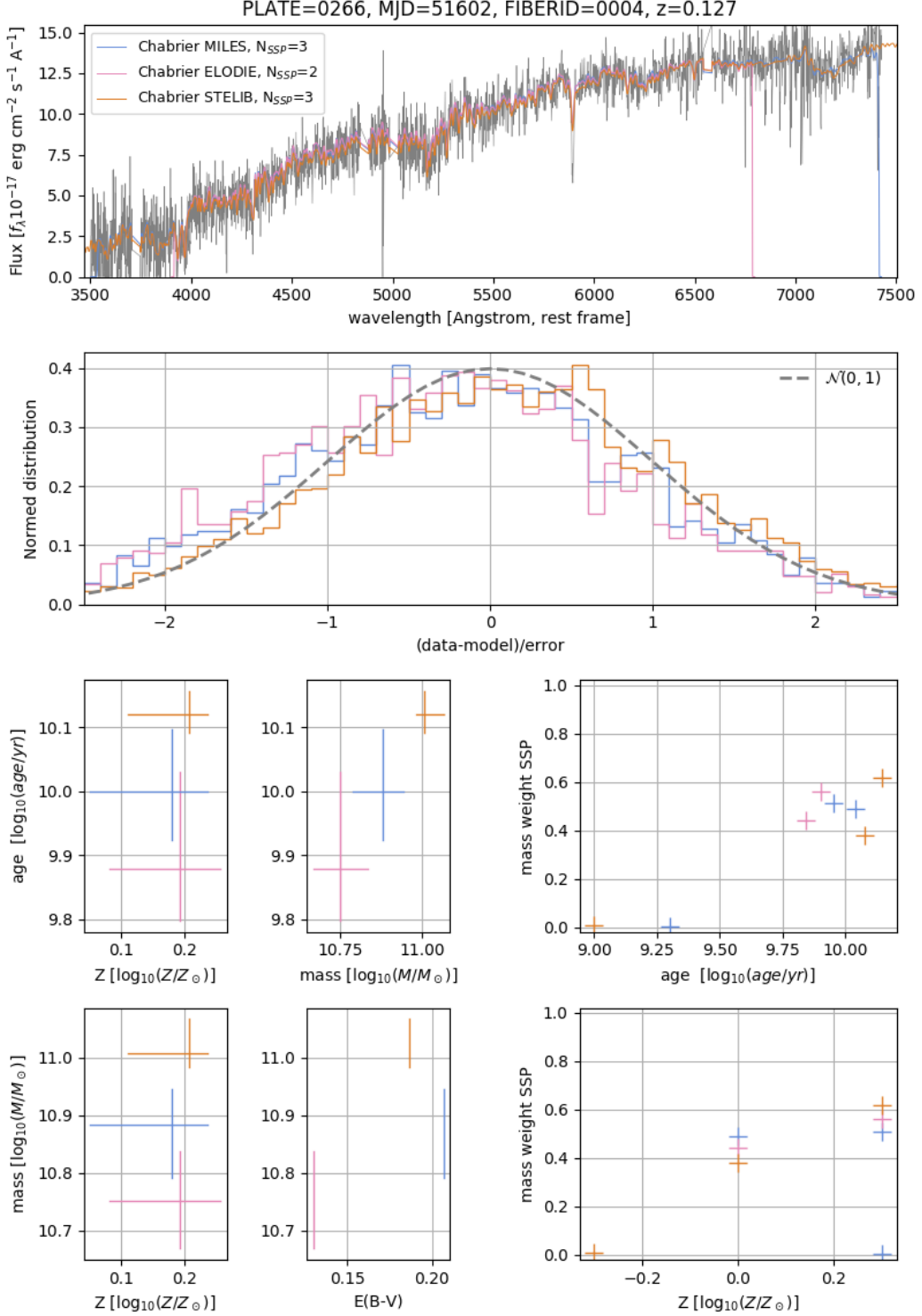


Fig. 2. Same as Fig. 1 for a galaxy spectrum randomly taken from the first BOSS plate, namely plate=3586, mjd=55181, fiberid=3, featuring a galaxy at redshift 0.588. It has a S/N around the 4000Å break of 3.1. The results point overall towards a metallicity around solar, an age larger than a few billion years, a larger reddening and a stellar mass around $10^{11} M_{\odot}$. The fit is dominated by a single old SSP with solar metallicity. The uncertainties on the derived parameters are larger than in the SDSS case of Figure 1.

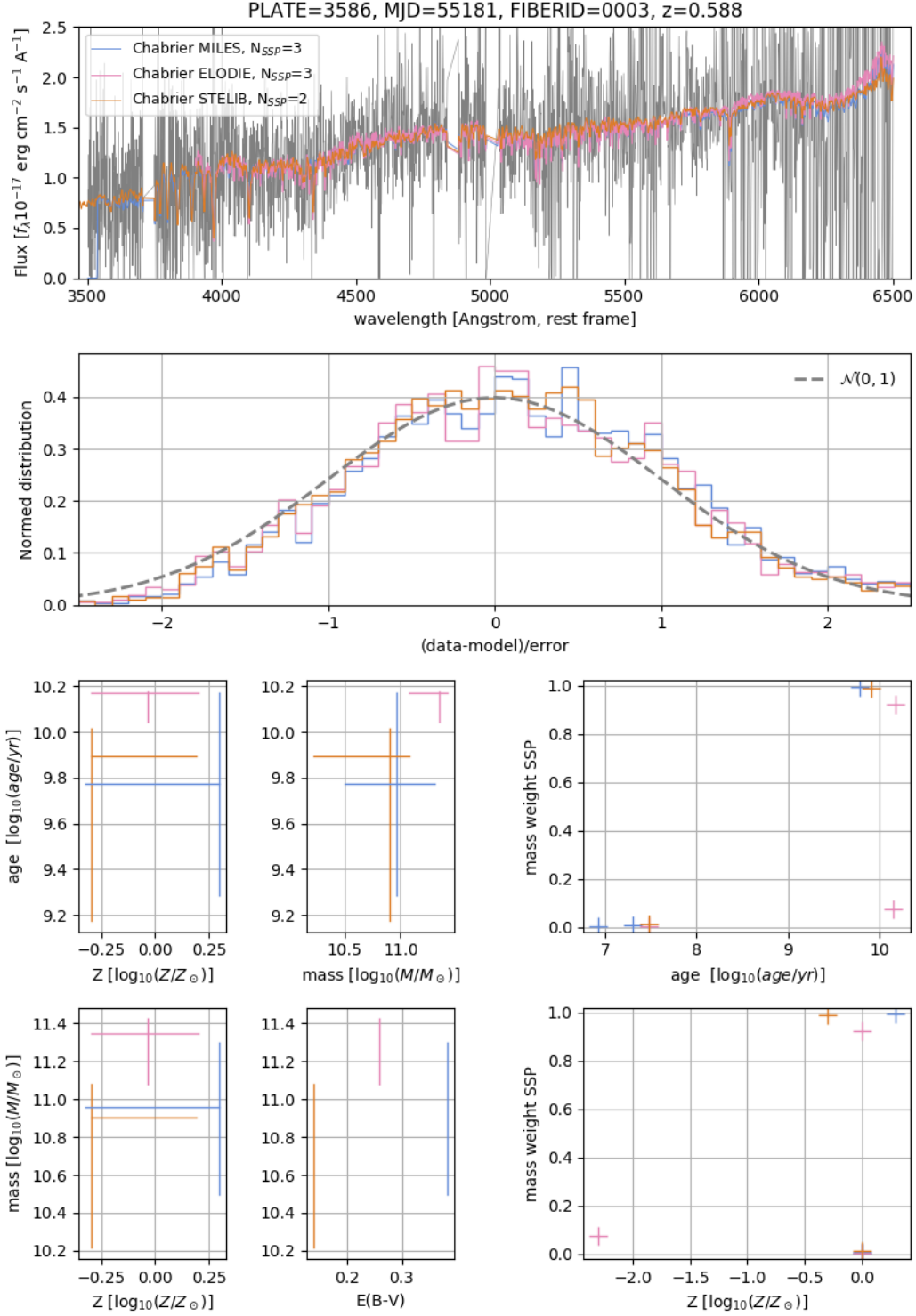
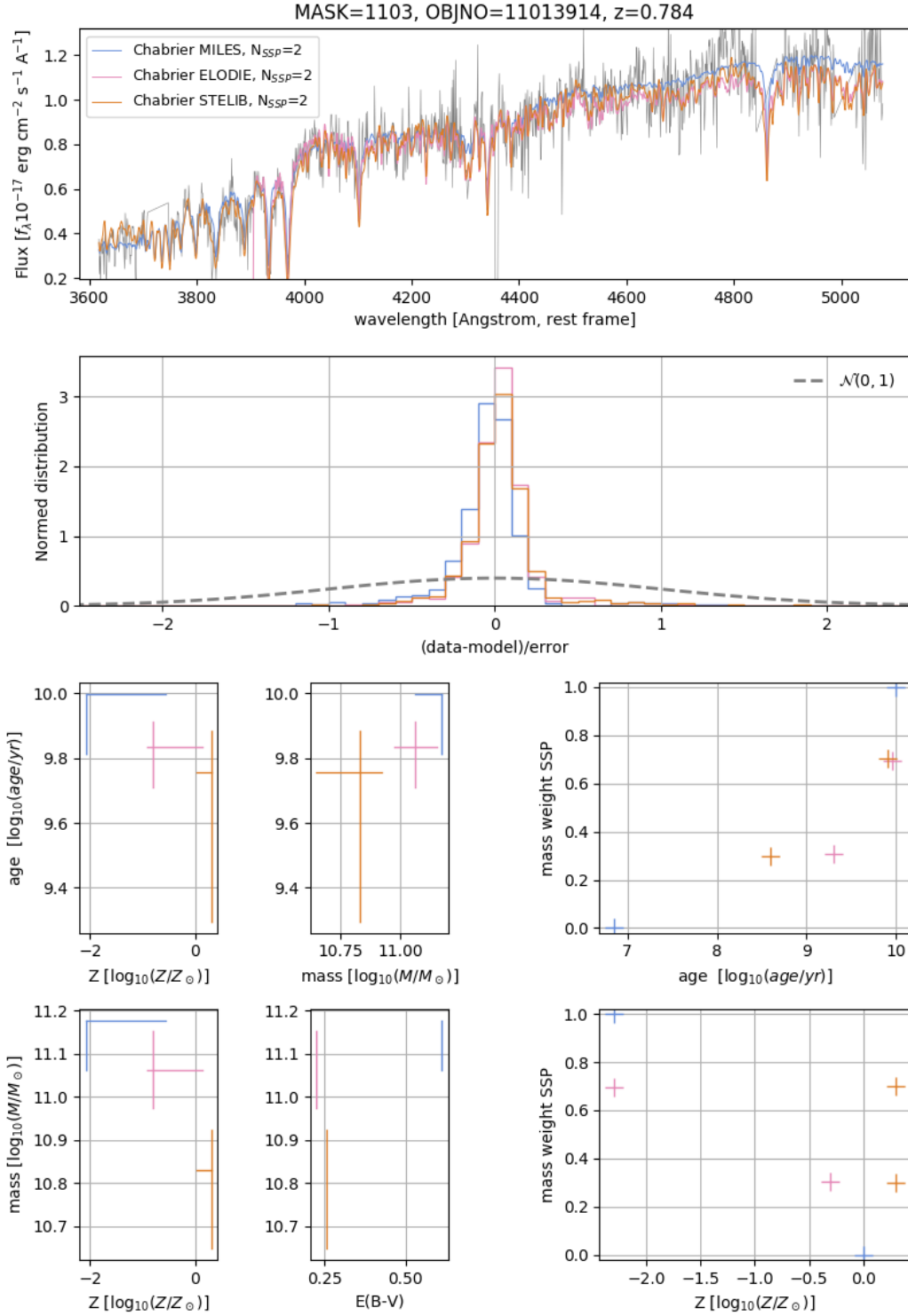


Fig. 3. Same as Fig. 1 for the DEEP2 spectrum at mask=1103 and objno=11013914. It features a galaxy at redshift 0.784. It has a median S/N of 5.4. The results point overall towards a metallicity value of $10^{-1}Z_{\odot}$, an age of $10^{9.9}$ yr, $E(B-V)$ between 0.2 and 0.6 and a mass around $10^{11}M_{\odot}$. The decomposition in SSPs with the ELODIE library suggest a combination of a young and an old SSPs both with sub solar metallicities.



4. Resulting galaxy parameters

In this section we describe the results of the fitting procedure, present statistics on the four main considered parameters.

Contents

4.1	Ages and metallicities	10
4.2	Dust and stellar masses	10
4.3	Star Formation history	12

4.1. Ages and metallicities

We show in Fig. 4 how each dataset occupies the input parameter space of ages and metallicities. SDSS galaxies mostly occupy the space of old and metal rich populations at low redshift ($z \sim 0.1$). eBOSS due to its higher mean redshift ($z \sim 0.5$) samples slightly younger ages and slightly lower metallicities. DEEP2 occupies the complementary space of lower ages and metallicities at higher redshifts ($z \sim 0.8$). In the DEEP2 case, it seems that a certain number of fits occupy the lowest metallicity edge of the parameter space, meaning these values may be not very well constrained. The young ages found for a fraction of galaxies using STELIB models might just be an artefact of the models

Regarding the input stellar library, the age/metallicity distributions obtained using models based on the MILES and the ELODIE libraries are overall similar, as already discussed on a smaller sample by Wilkinson et al. (2017). For the eBOSS sample (second row) lying at higher redshift and based on a different target selection, ELODIE-type models give a distribution of metallicities stretching towards sub-solar values while MILES-based models remain more concentrated at solar metallicities. The STELIB library grants a smaller coverage in metallicity hence model results are confined within half-solar and twice-solar in chemical composition. Because of the smaller range of input metallicity and due to the age metallicity degeneracy, the range in ages found using STELIB-based models is larger and extend to younger ages with respect to the other two models. These results highlight how much galaxy evolution findings depend on the assumed model frame used to interpret galaxy spectra.

Quantitative comparisons between the obtained ages and metallicities are shown in Figures 5 and 6, described in the next paragraphs.

Stellar age

We find that - at fixed stellar library - variations in the IMF assumed in the models give ages that remain always consistent within 1σ . On the contrary, at fixed IMF, variations in the input stellar library produce the largest difference among models. While the ages obtained with MILES and ELODIE-type models (at a fixed Chabrier IMF) are consistent within 1σ with each other in both the SDSS and eBOSS samples, those obtained with STELIB are discrepant from the other two sets of models due to the small coverage in metallicity of the library. Fig. 5 shows the distribution of age difference normed by their 1σ uncertainties when varying the input libraries, ELODIE, MILES and STELIB (at fixed Chabrier IMF). Absolute values of age for the sample galaxies are presented in Section 5.

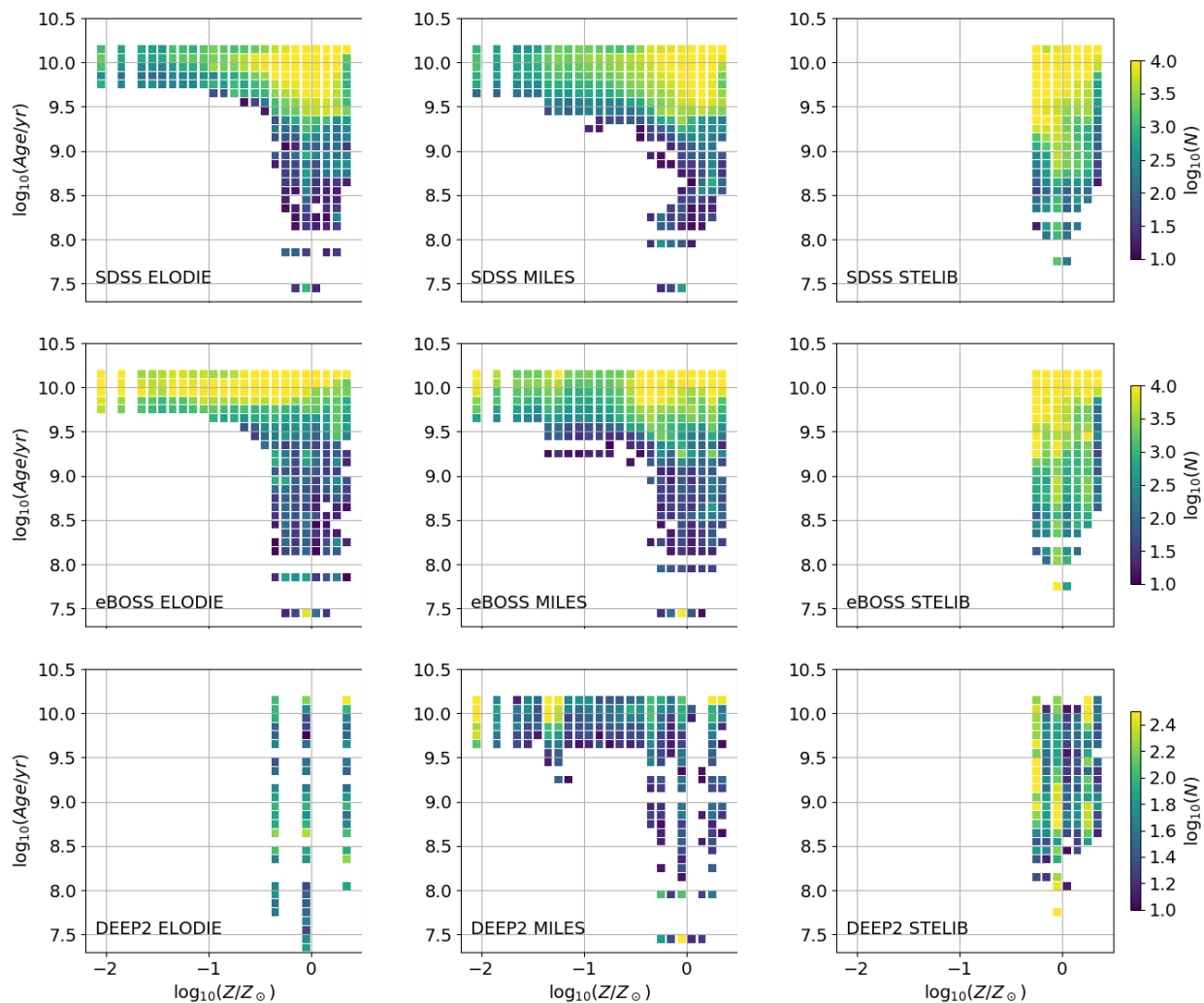
Stellar metallicity

At fixed IMF, the metallicities derived with models based on different stellar libraries are not always consistent, but the result also depends on the galaxy sample. Fig. 6 shows the distribution of the difference of metallicity normed by the uncertainty on the parameter when varying the libraries: ELODIE, MILES, STELIB (for a Chabrier IMF). In case of the SDSS sample, metallicities are nearly consistent. The distribution shows a small systematic shift, but the overall width is comparable to that of a Gaussian. For the DEEP2 sample, errors are very large, hence the distribution seems consistent, but the parameter metallicity is quite unconstrained. For the eBOSS sample, on the other hand, there are systematic deviations when comparing either MILES and ELODIE or MILES and STELIB. The distribution is broader than the Gaussian meaning there is a disagreement between the parameter estimation. This is the case also for the MILES vs ELODIE comparison, even if the two stellar libraries offer a similar metallicity coverage. Hence, the disagreement is not just simply due to the different coverage in input parameters. We thus warn the future user to be cautious when using the metallicity parameters fitted on the eBOSS data. Absolute values of metallicity for the sample galaxies are presented in Section 5.

4.2. Dust and stellar masses

Similarly to the age-metallicity degeneracy there exists a dust-age degeneracy which creates a dust-mass degeneracy. Both a young and very dusty model or an old dust-free model can provide a good description of the same spectrum (Renzini 2006). Thus for an old and dust free galaxy, its stellar mass could be significantly underestimated (Pforr et al. 2012). In specific cases, like Maraston et al. (2013), where they analyzed the sample of massive galaxies in SDSS-DR12, they assumed dust-free models to avoid this bias. Indeed, these galaxies should not be dominated by a young stellar population. In our analysis, because the galaxy populations considered cover a large redshift range and a variety of different galaxy types, we choose to fit for dust in the analysis. In Fig. 7 we show how each dataset occupies the input parameter space of dust and stellar mass. The distributions obtained with ELODIE and MILES are similar, with a tendency for MILES-based models to find a larger fraction of dusty galaxies at low stellar masses

Fig. 4. 2-D age/metallicity histograms for the SDSS (top row), eBOSS (middle row) and DEEP2 (bottom row) data in the 3 library setups, ELODIE, MILES and STELIB (rows from left to right) for the Chabrier IMF. These show how each library samples the age-metallicity plane. The difference between surveys come from the different redshift range, but also from targeting different type of galaxies. Note that the axis of the colour maps are different for DEEP2.



($M < 10^9 M_{\odot}$). Fits done with the M11-STELIB models favour a lower dust attenuation for the eBOSS sample due to the lack of low metallicity coverage in these models. DEEP2 galaxies seem to cluster on the low $E(B-V)$ side, although this may be due to the small wavelength coverage of the sample. Note that due to a larger volume and a preselection to include only massive galaxies, eBOSS seems to contain more massive galaxies than SDSS although the mean redshift is greater. We directly compare the stellar mass and $E(B-V)$ values obtained in the next two paragraphs and on Figs. 8 ($E(B-V)$), 9 (stellar mass), 10 (stellar mass).

Dust

The assumed library induces a noticeable difference in the retrieved $E(B-V)$. Fits done with M11-STELIB (largest wavelength coverage) provide on average lower values of attenuation than those based on M11-MILES and M11-ELODIE (smallest wavelength coverage), see Fig. 8. SDSS and eBOSS have a larger wavelength coverage than the models so that the models are the limiting factor. DEEP2 has a limited wavelength coverage so this directly impacts the ability of the software to constrain $E(B-V)$ and in most cases it is 0. As expected, the IMF has no impact on the derived $E(B-V)$.

Stellar mass

Stellar masses obtained with the Kroupa IMF are systematically smaller than those obtained with either a Chabrier or a Salpeter IMF. Fig. 9 shows the difference in stellar masses obtained when initial mass functions are varied, for the fixed M11-MILES models. The systematic difference in the inferred masses due to the assumed IMF is larger than the statistical uncertainty on stellar mass. Fig. 10 shows the difference in the stellar masses obtained when the stellar library is varied. It shows that changing library also

Fig. 5. Normed distribution (area is equal to 1) of the difference in age weighted by its 1σ uncertainty obtained when assuming different libraries and fixed IMF to Chabrier for the DEEP2 (left), the SDSS (middle) and eBOSS (right) samples. The difference between ages obtained with the MILES and the ELODIE is shown with a blue solid line. The difference between ages obtained with the STELIB and the ELODIE is shown with a pink solid line. This Figure quantifies the differences seen qualitatively between libraries in Fig. 4. The Gaussian distribution (orange dashed line) shows the width of the distribution expected if the ages derived agree within errors. MILES and ELODIE ages are in good agreement but STELIB and ELODIE ages disagree.

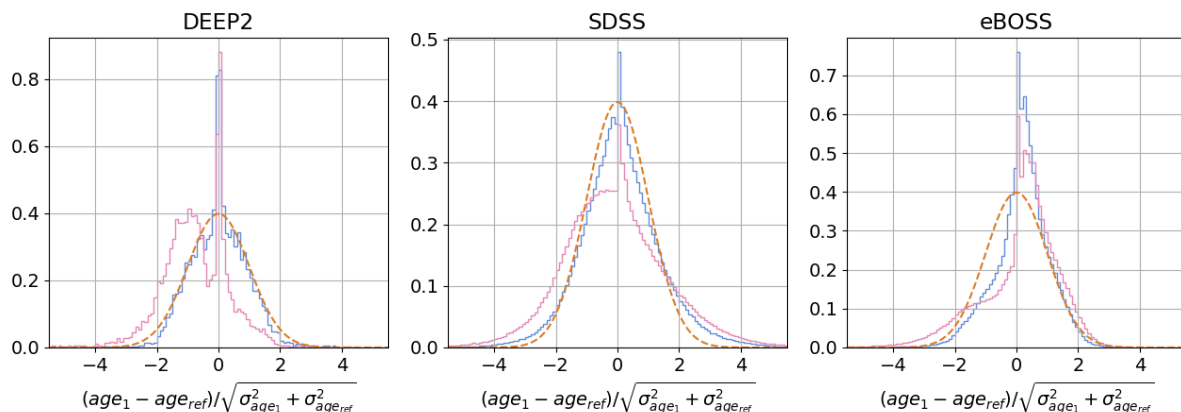
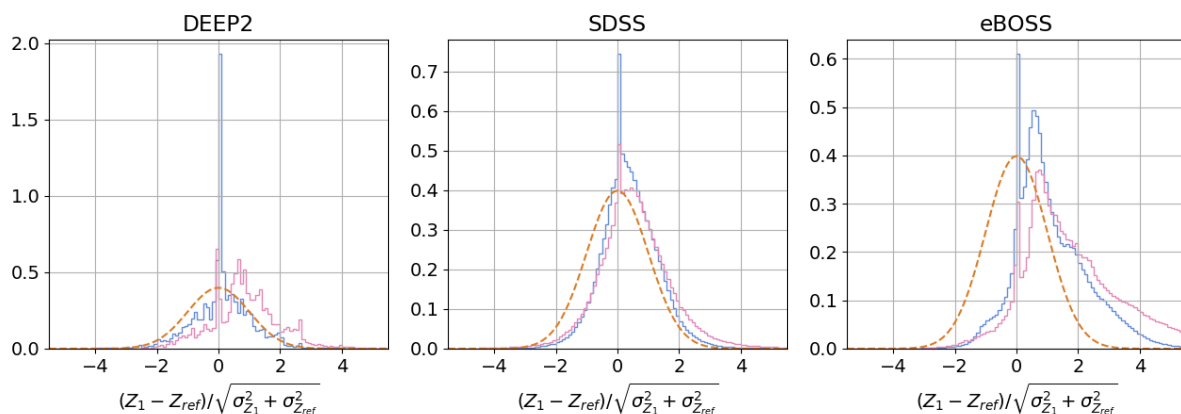


Fig. 6. Same as Fig. 5 for the stellar metallicity. The difference between metallicities obtained with the MILES and the ELODIE is shown with a blue solid line. The difference between metallicities obtained with the STELIB and the ELODIE is shown with a pink solid line. The Gaussian distribution (orange dashed line) shows the width of the distribution expected if the ages derived agree within errors.



induces systematic changes in the stellar mass that are larger than the statistical uncertainty on the stellar mass. The masses obtained with the Salpeter (Kroupa) IMF are on average 0.08 to 0.1dex (-0.02dex) more (less) massive than with the Chabrier IMF.

Fig. 10 summarises our analysis by assessing the consistency of all derived parameters simultaneously (at fixed IMF) when varying input library. We find that models based on either MILES and ELODIE give statistically consistent sets of galaxy parameters in case of SDSS and DEEP2 while for the eBOSS sample, the parameters derived with the various models are not consistent. Likewise, parameters derived using STELIB and ELODIE models are not consistent independently of the galaxy sample.

4.3. Star Formation history

In cases of high signal to noise (> 20), the star formation history can be reconstructed. Fig. 1 shows a low redshift galaxy observed at high signal to noise. The third panel on the third row shows the mass weight of each SSP. It indicates that this galaxy spectrum could be explained by the combination of two 10 Gyr old components with a solar metallicity contributing to more than 90% of the mass and a ~ 1.5 Gyr old component with a sub solar metallicity contributing to the remaining 10%. We show how SSPs components are distributed in parameter space in Sec. 5.

Fig. 7. Dust - stellar mass 2d-histograms for the SDSS (top row) eBOSS (middle row) and DEEP2 (bottom row) data in the 3 library setups: columns ELODIE, MILES, STELIB for the Chabrier IMF.

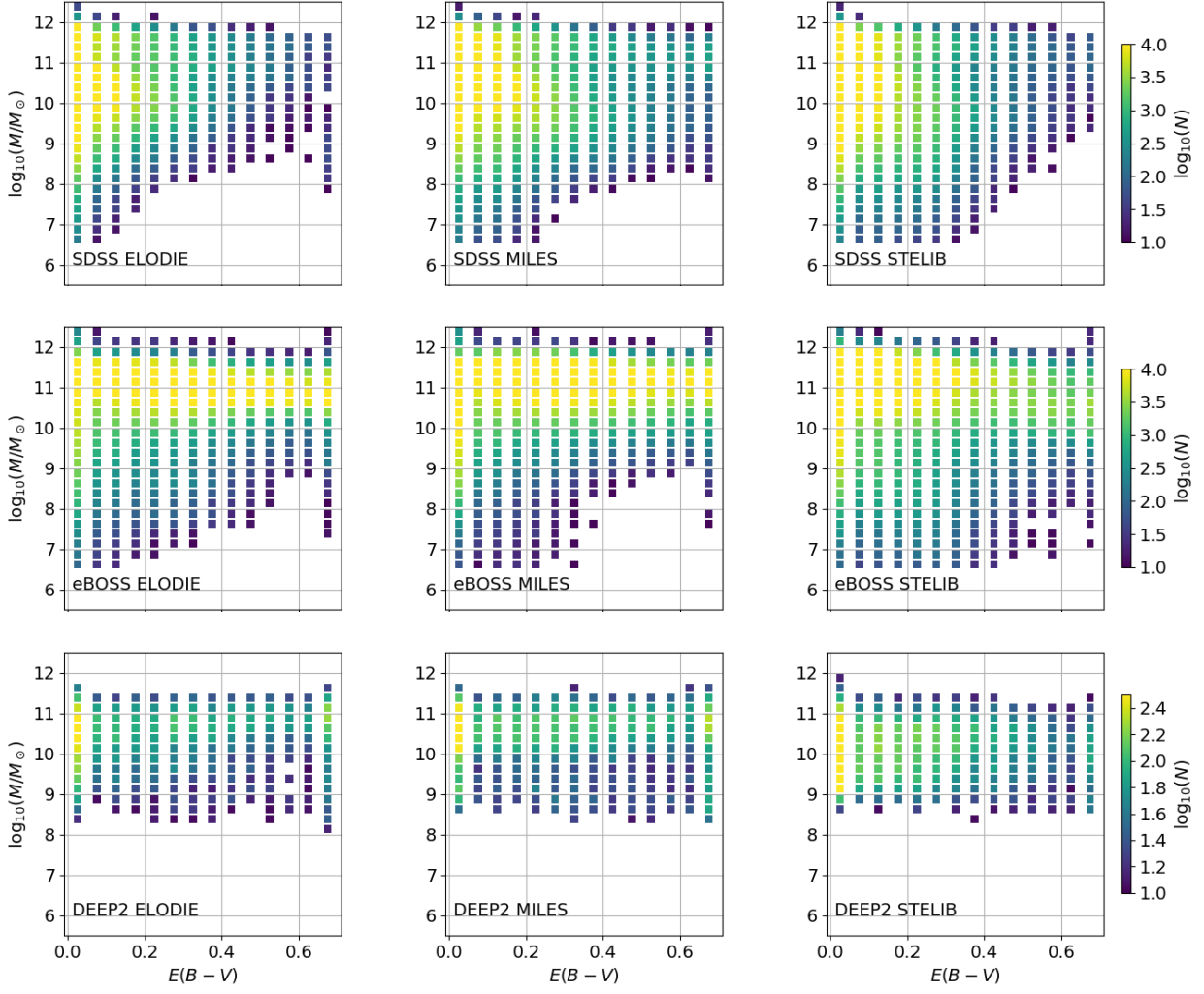


Fig. 8. Distribution of the difference of $E(B-V)$ when varying the libraries: ELODIE, MILES, STELIB (fixed IMF: Chabrier). Due to different wavelength coverage in each library, the $E(B-V)$ values measured differ by up to 0.2 dex. The difference between $E(B-V)$ obtained with the MILES and the ELODIE is shown with a blue solid line. The difference between $E(B-V)$ obtained with the STELIB and the ELODIE is shown with a pink solid line.

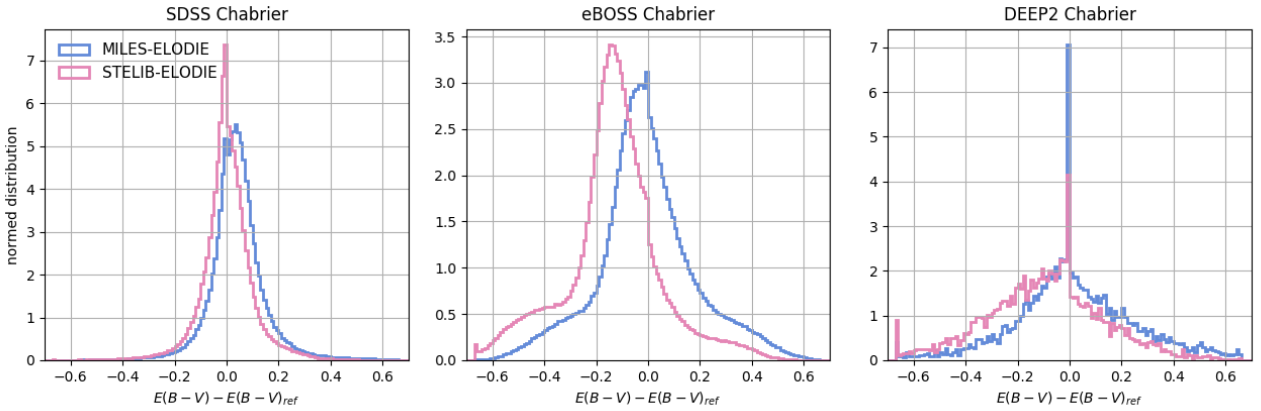


Fig. 9. Comparison of stellar masses obtained at the fixed M11-MILES model and varying the IMF, for the three samples: SDSS (left); eBOSS (middle); DEEP2, (right). Stellar masses are systematically different, as expected. Kroupa is systematically less massive than Chabrier, and both Kroupa and Chabrier are systematically less massive than Salpeter. The difference between stellar masses obtained with the Kroupa and the Chabrier is shown with a blue solid line. The difference between stellar masses obtained with the Salpeter and the Chabrier is shown with a pink solid line.

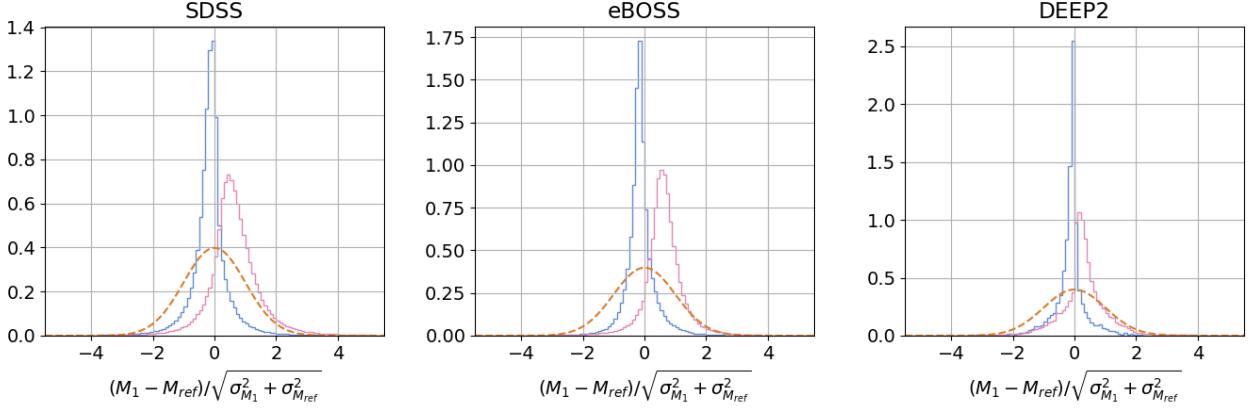


Fig. 10. Global comparison of stellar masses obtained with varying the assumed model (at a fixed Chabrier IMF). If the obtained distribution is narrower than a normal distribution (depicted with the line 'N(0,1)') then measurements agree within errors. The difference between stellar masses obtained with the MILES and the ELODIE is shown with a blue solid line. The difference between stellar masses obtained with the STELIB and the ELODIE is shown with a pink solid line. The difference between stellar masses obtained with the STELIB and the MILES is shown with an orange solid line.

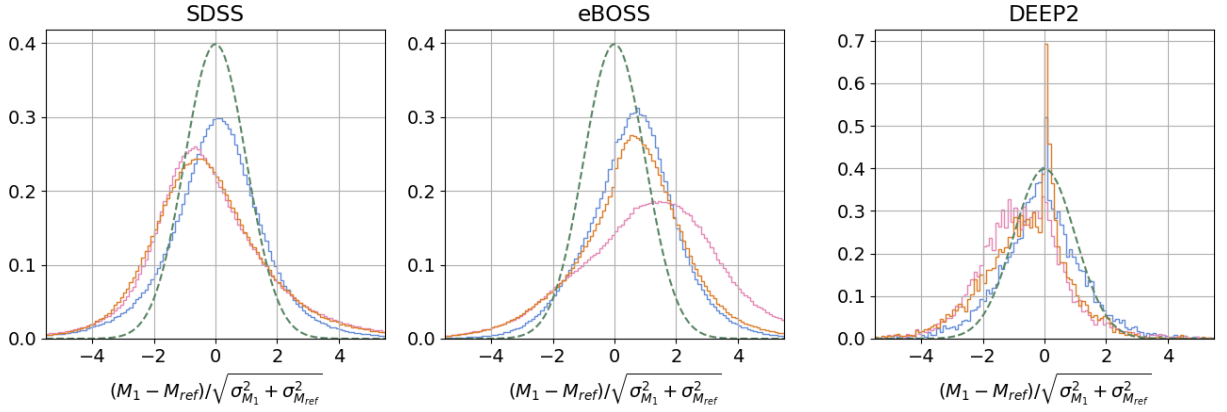
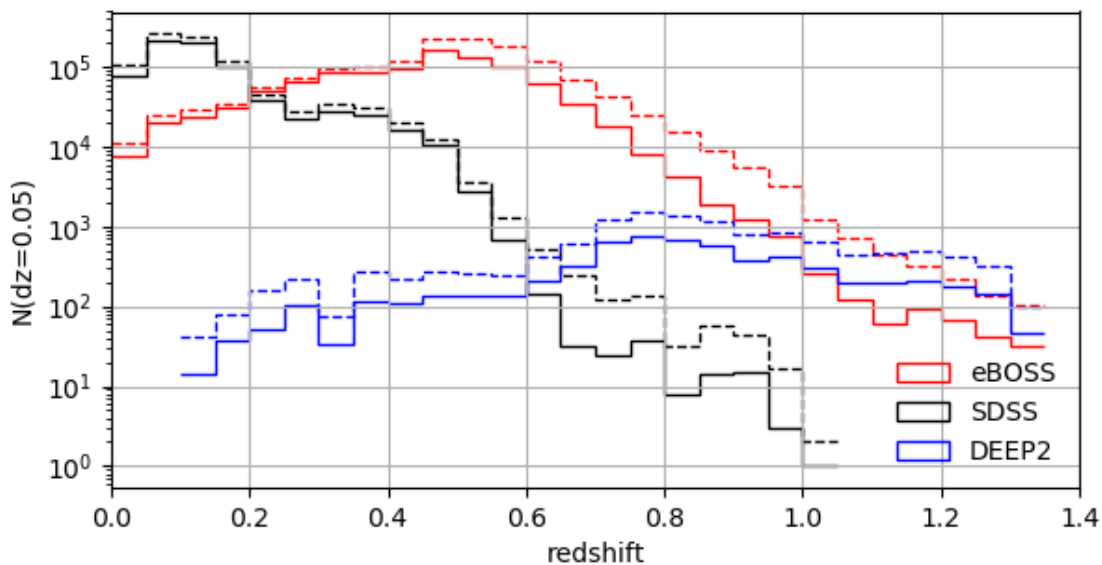


Fig. 11. Galaxy redshift distributions, where galaxies with stellar mass constrained within ± 0.2 dex are shown as solid lines, and within ± 0.4 dex as dashed lines. Stellar masses used here are obtained using M11-ELODIE and refer to the Chabrier IMF.



5. Results

Our results span a large range in redshift ($0 < z < 1.3$) and stellar mass ($7 < \log M^*/M_\odot < 12$) and can be used for a variety of galaxy evolution studies. Fig. 11 shows the redshift distribution of the galaxies with determined stellar properties. Fig. 12 shows their distribution in the stellar mass vs redshift plane. Detailed figures for the plotted quantities are given in Tables 1 and 2.

In the following, we first describe the overall results, e.g. number of galaxy with fitted stellar properties, redshift distribution and parameter - age, metallicity and stellar mass - distributions. We then discuss how the uncertainty of the fitted parameters is related to observational parameters.

5.1. SDSS and eBOSS

The SDSS+eBOSS specObjAll file contains 1,843,200 + 3,008,000 spectra, respectively, among which 950,705 and 1,759,362 are classified as galaxies. Among the latter, 948,259 (99.7%) and 1,759,362 (100%) could be run through our model spectral fitting, see Table 1. The small fraction of missing data in SDSS is due to the fact that we only use the data from the observational run dedicated to galaxy targets (the run is named ‘26’). Indeed in the observational runs dedicated to stellar targets (runs named ‘103’ and ‘104’) some galaxies might have been mistaken for stars i.e. this sample is contaminated by galaxies. We will include the runs 10 and 104 in future releases. More than 95% of SDSS and eBOSS galaxies have their output stellar mass constrained i.e. $0 < M^* - \sigma_M < M^* + \sigma_M < 10^{14} M_\odot$. The remaining 5% have returned fitted parameters but they are consistent with a stellar mass of 0. We call these fits ‘unconstrained’.

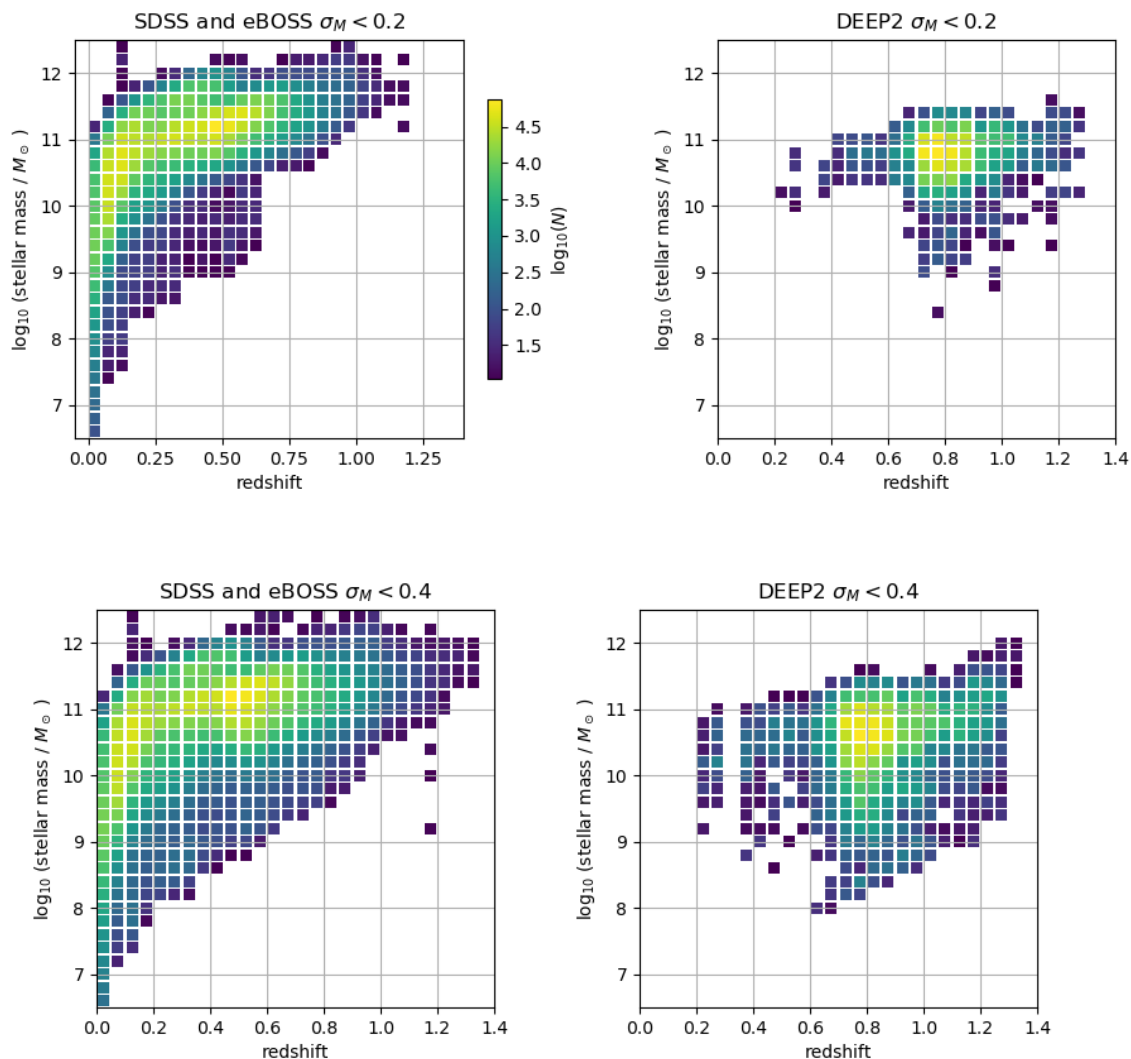
For each observed galaxy spectrum we provide models of the continuum in up to 9 combinations of stellar population model and IMF.

This is the first full spectral fitting release of the BOSS+eBOSS high-redshift extension of SDSS which provide stellar population parameters. Previous work performing spectral fitting was based on a PCA approach (Chen et al. 2012) aimed at optimizing the stellar mass determination, and for which stellar parameters were not provided.

5.2. DEEP2

The DEEP2 catalog contains 21,273 galaxies in the redshift range $0.7 < z < 1.2$, see Table 2. The fitting routine converges for all. However, due to their generally low SNR, the fraction of spectra for which the stellar mass parameter obtained has an uncertainty smaller than $\sigma_{\log_{10} M} < 0.4$ dex, is small, amounting to less than 40%. Among the 21,273 spectra, 30% have a SNR below 1 and only 10% above 2. Only 200 objects have a SNR above 5. This sample will not allow us to explore detailed stellar population properties. This distribution of SNRs explains why only roughly 35% (15%) have a stellar mass constrained within 0.4 (0.2) dex (Table 2). From the mock exercises of Wilkinson et al. (2017) (e.g. Figures 12-15) we know that stellar masses can be reasonably recovered down to low SNRs ($S/N \sim 5$), but the uncertainty is high and with DEEP2 we are dealing with even lower SNRs. We regard the DEEP2 spectral fitting analysis as an extreme example to explore the boundaries of full spectral fitting.

Fig. 12. Stellar mass vs redshift distributions for the three considered galaxy samples distinguishing between those whose stellar mass is constrained within ± 0.2 dex (upper panels) and ± 0.4 dex (lower panels). Stellar masses shown here are obtained using M11-ELODIE and refer to the Chabrier IMF.



5.3. General findings as a function of parameters.

Depending on fitting setup, between 81 and 96% of the fits give constrained parameters for the SDSS+eBOSS data and between 22 and 36% for the DEEP2 data. For example, in the case M11-MILES and a Chabrier IMF, 80% (70%) of the SDSS (eBOSS) data stellar masses are constrained to the 0.2 dex level, where by ‘constrained’ we mean that the statistical errors are smaller than 0.2 dex on the stellar mass.

For the DEEP2 data, due to the intrinsic faintness of the spectra and the much lower SNR of the continuum, we could tightly constrain stellar parameters for only about 10% of the sample. Exact numbers are available in Tables 1, 2.

In SDSS+eBOSS, un-constrained fits are dominated by spectra with low signal to noise ratio ($< 1 - 2$) and by a fraction of QSOs that were mis-classified as galaxies by the automated pipeline. In the DEEP2 data, the un-constrained fits are split into two components: the restricted wavelength coverage of the spectra; very low signal to noise ratio in the continuum ($\sim 0.1-1$) (Redshift determined with emission lines only).

In any case, the sample with fitted properties is not a clean subset of the parent catalogs, rather it is a biased subsample of the parent catalogs. It is biased as a function of position on the sky and magnitude. Fig. 13 shows the distribution on the sky of galaxies in the SDSS and eBOSS catalogs and the distributions of galaxies for which the stellar mass parameters is determined to better than 0.2 dex. We note differences in density of points. The gaps correlate with specific plates that have overall a smaller signal to noise. Furthermore, the distribution in magnitude of the galaxies with stellar mass parameter determined to better than 0.2 dex is not a fair sub sample of the complete galaxy population, in particular towards the faint end, see Fig. 14 that shows the fraction of constrained fits as a function of the SDSS r -band magnitude.

Table 1. Summary table of observed spectra and fit results for SDSS and BOSS. The Table is divided in four sectors. The first line in each subset gives the total number of spectra available in the survey and how many of them are considered as galaxies. The assumed fitting setup (model and IMF) is given in the first 2 columns. The third column gives the number of galaxies for which the obtained stellar mass is non zero. The last two columns gives the number of galaxies for which the stellar mass parameter is constrained within less than 0.4 dex and 0.2 dex, respectively. The number in parenthesis give the percentage relative to the total number of galaxies.

eBOSS DR14: 1,759,362 galaxies				
IMF	Library	$M > 0$	$\sigma_{\log_{10} M} < 0.4$ dex	$\sigma_{\log_{10} M} < 0.2$ dex
Chabrier	ELODIE	1758635 (100.0)	1427861 (81.2)	980810 (55.7)
Chabrier	MILES	1758819 (100.0)	1529842 (87.0)	1237575 (70.3)
Chabrier	STELIB	1758934 (100.0)	1466376 (83.3)	1217235 (69.2)
Kroupa	ELODIE	1758635 (100.0)	1446616 (82.2)	1012728 (57.6)
Kroupa	MILES	1758819 (100.0)	1556522 (88.5)	1278732 (72.7)
Kroupa	STELIB	1758934 (100.0)	1490832 (84.7)	1252335 (71.2)
Salpeter	ELODIE	1758635 (100.0)	1467855 (83.4)	1047431 (59.5)
Salpeter	MILES	1758819 (100.0)	1583900 (90.0)	1351031 (76.8)
Salpeter	STELIB	1758934 (100.0)	1504425 (85.5)	1270344 (72.2)
SDSS DR14: 948,259 galaxies				
IMF	Library	$M > 0$	$\sigma_{\log_{10} M} < 0.4$ dex	$\sigma_{\log_{10} M} < 0.2$ dex
Chabrier	ELODIE	938316 (99.0)	886081 (93.4)	729736 (77.0)
Chabrier	MILES	938317 (99.0)	901024 (95.0)	765905 (80.8)
Chabrier	STELIB	938317 (99.0)	882412 (93.1)	722856 (76.2)
Kroupa	ELODIE	938316 (99.0)	892330 (94.1)	760271 (80.2)
Kroupa	MILES	938317 (99.0)	905489 (95.5)	798735 (84.2)
Kroupa	STELIB	938317 (99.0)	890963 (94.0)	752197 (79.3)
Salpeter	ELODIE	938316 (99.0)	896355 (94.5)	774556 (81.7)
Salpeter	MILES	938317 (99.0)	909374 (95.9)	814850 (85.9)
Salpeter	STELIB	938317 (99.0)	894546 (94.3)	768726 (81.1)

Table 2. Same as Table 1 for DEEP2 and DEEP2 [On] galaxies. The last set shows the subset of the DEEP2 set that have a detection with a signal to noise ratio greater than 5 of the [On] emission line.

DEEP2 DR4: 21,273 galaxies $0.7 < z < 1.2$				
IMF	Library	$M > 0$	$\sigma_{\log_{10} M} < 0.4$ dex	$\sigma_{\log_{10} M} < 0.2$ dex
Chabrier	ELODIE	21268 (100.0)	6006 (28.2)	2798 (13.2)
Chabrier	MILES	21273 (100.0)	6934 (32.6)	3193 (15.0)
Chabrier	STELIB	21273 (100.0)	6823 (32.1)	1796 (8.4)
Kroupa	ELODIE	21268 (100.0)	6638 (31.2)	3031 (14.2)
Kroupa	MILES	21273 (100.0)	7274 (34.2)	3548 (16.7)
Kroupa	STELIB	21273 (100.0)	7394 (34.8)	2163 (10.2)
Salpeter	ELODIE	21268 (100.0)	7008 (32.9)	3162 (14.9)
Salpeter	MILES	21273 (100.0)	7565 (35.6)	3752 (17.6)
Salpeter	STELIB	21273 (100.0)	7644 (35.9)	2435 (11.4)
DEEP2 DR4: 15,498 [On] galaxies $0.7 < z < 1.2$				
IMF	Library	$M > 0$	$\sigma_{\log_{10} M} < 0.4$ dex	$\sigma_{\log_{10} M} < 0.2$ dex
Chabrier	ELODIE	15493 (100.0)	3444 (22.2)	1431 (9.2)
Chabrier	MILES	15498 (100.0)	4090 (26.4)	1822 (11.8)
Chabrier	STELIB	15498 (100.0)	3975 (25.6)	944 (6.1)
Kroupa	ELODIE	15493 (100.0)	3903 (25.2)	1529 (9.9)
Kroupa	MILES	15498 (100.0)	4267 (27.5)	1960 (12.6)
Kroupa	STELIB	15498 (100.0)	4390 (28.3)	1108 (7.1)
Salpeter	ELODIE	15493 (100.0)	4184 (27.0)	1619 (10.4)
Salpeter	MILES	15498 (100.0)	4545 (29.3)	2123 (13.7)
Salpeter	STELIB	15498 (100.0)	4559 (29.4)	1228 (7.9)

Statistical error on derived parameters

The statistical uncertainty on the stellar age, stellar metallicity and stellar mass is estimated using the full probability distribution function of the parameters derived during the fit. We provide the 1 and 2 σ uncertainties. Fig. 15 shows the distribution of the 1 σ uncertainties obtained. Although uncertainties on age and metallicity can be quite high, the uncertainty on the stellar mass remains contained.

Fig. 13. Distribution on the sky of galaxies in the SDSS (top left) and eBOSS (top right) catalogs. All panels have the same dot size and transparency level applied. The second line shows the distribution of galaxies for which the stellar mass parameters was determined to better than 0.2 dex. In the SDSS bottom left panel, we see small gaps that are not visible in the top left panel e.g. around R.A.=350°. In the eBOSS bottom right panel, we see that the stripe in $40^\circ < Dec. < 60^\circ$ is less dense than in the top right panel.

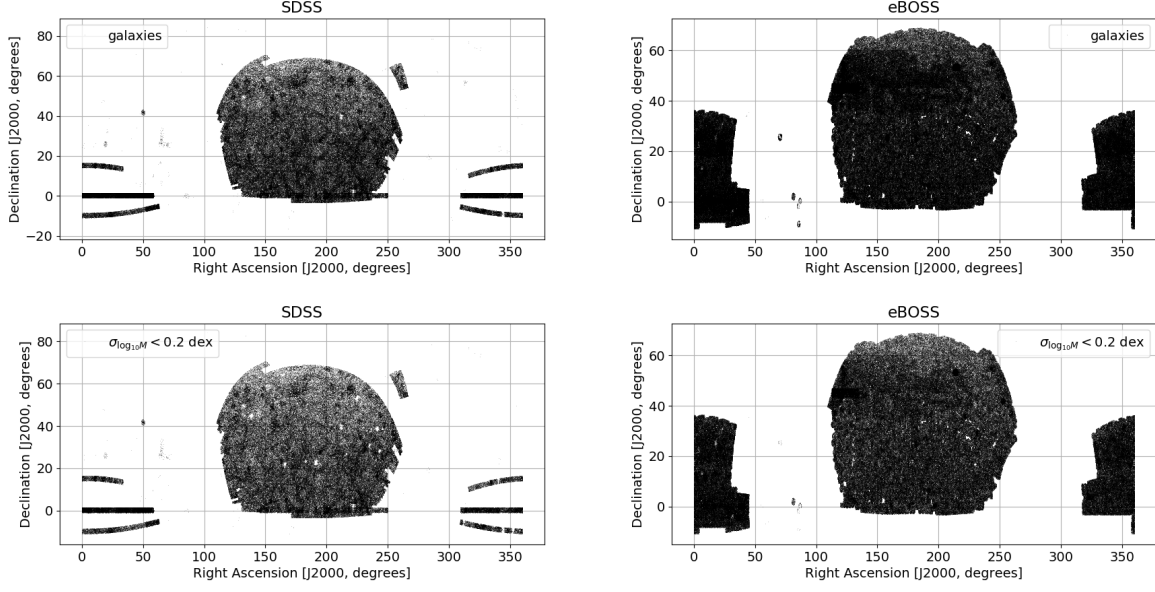


Fig. 14. Ratio between the number of galaxies for which the stellar mass parameter was determined to better than 0.2 (0.4) dex and the complete galaxy catalog in bins of SDSS r -band model magnitude (when available) for the SDSS catalog (left) and the eBOSS catalog (right). As expected, at the faint ends the fraction of galaxies with accurate stellar mass determinations drops.

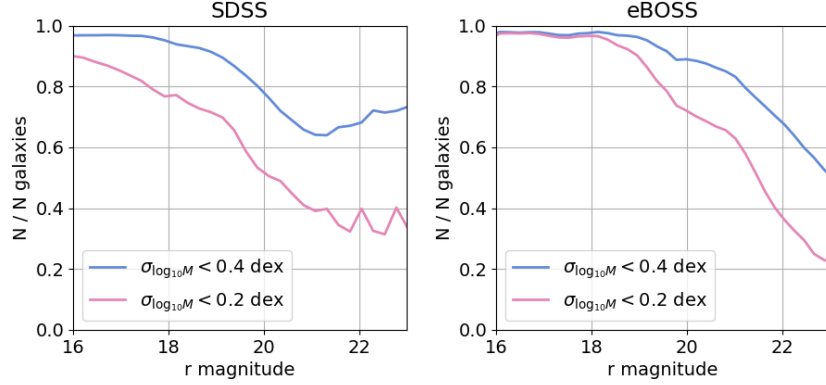


Fig. 15. Distributions of the 1σ errors on the stellar parameters: age (left), metallicity (middle), mass (right).

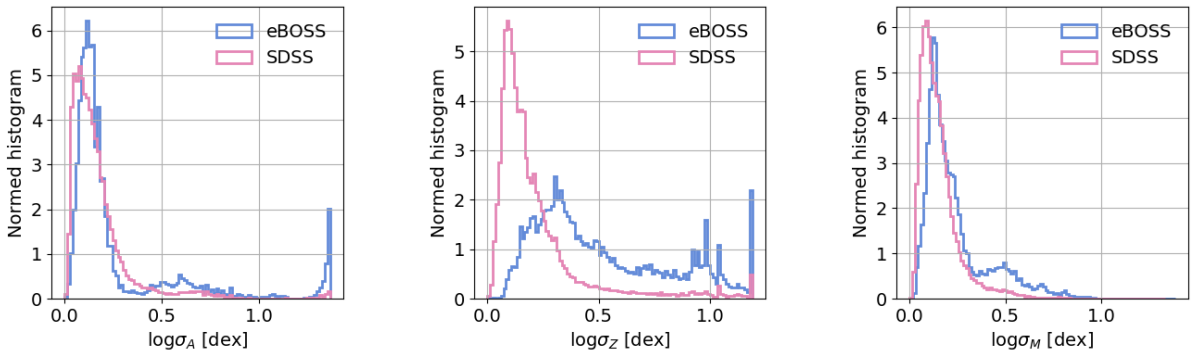
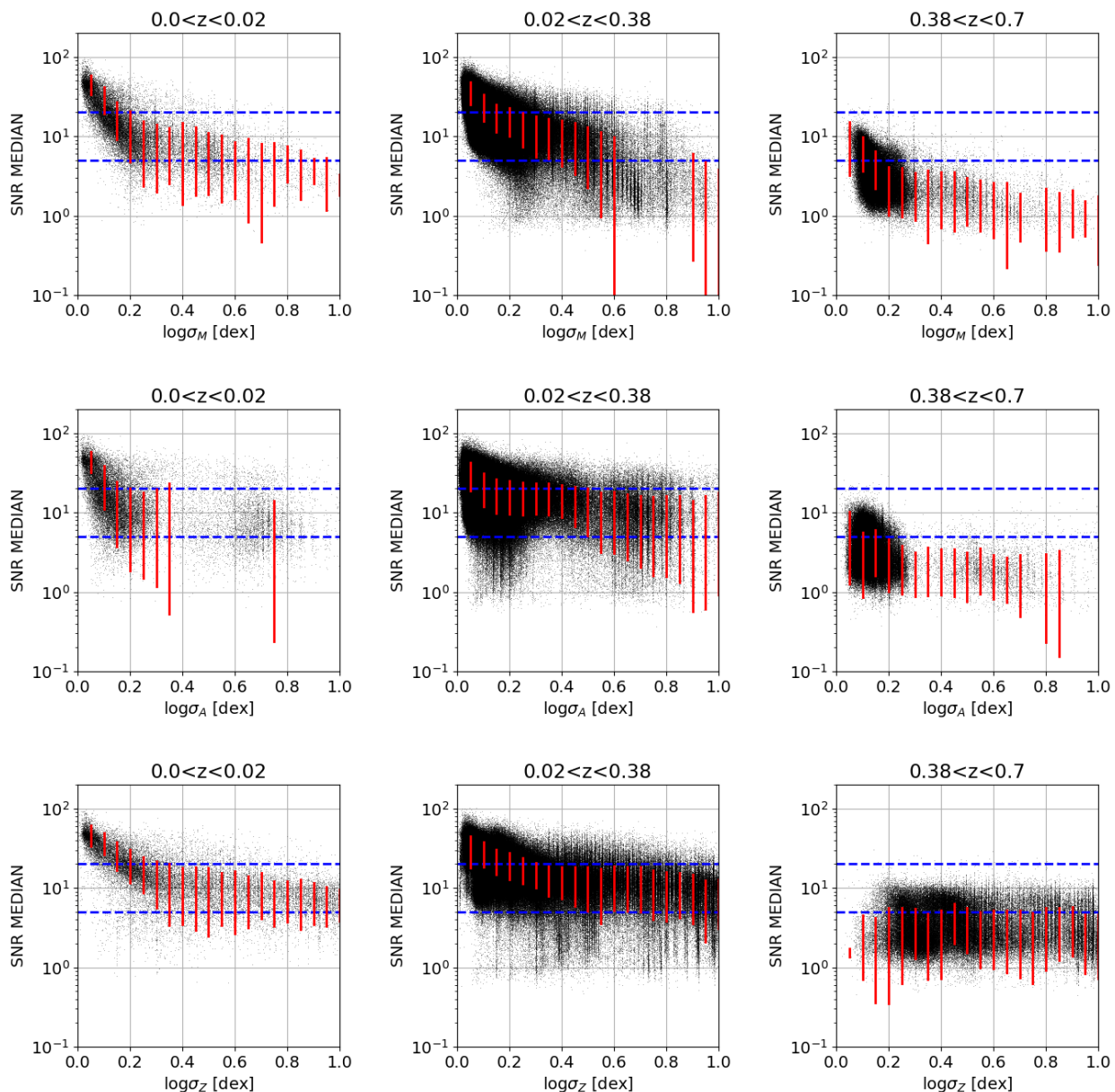


Fig. 16. Individual median signal to noise ratio in the SDSS+eBOSS spectra around the 4000 Angstrom break v.s. uncertainty on the stellar mass (top row), stellar age (middle row), stellar metallicity (bottom row). Each column shows a different redshift range. The red dashed show the mean and dispersion of the data binned along the x-axis.



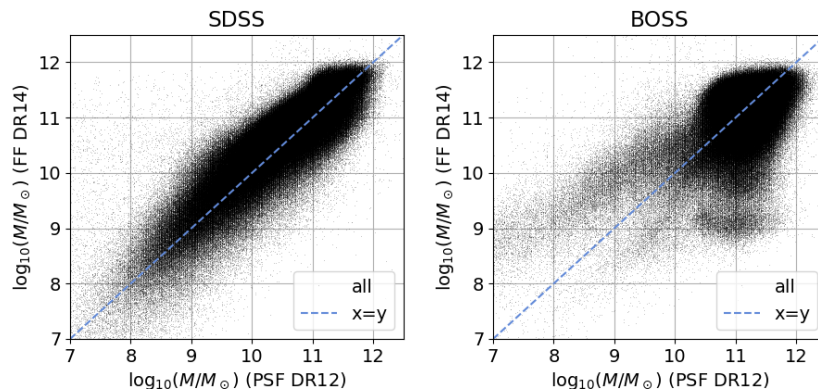
As in Wilkinson et al. (2017), we find that the uncertainties are mainly driven by the average signal-to-noise per pixel in the spectra in the band where information is localized (roughly $3800\text{-}5500\text{\AA}$). Fig. 16 shows the median signal to noise ratio in the spectrum around the 4000 Angstrom break v.s. uncertainty on the stellar mass, stellar age and stellar metallicity.

For spectra with large error on the stellar mass, one should be cautious, and combine this measurement with stellar masses (and other parameters in general) based on broad band magnitudes SED fitting (e.g. Maraston et al. 2013, for the same galaxies). In some sense, our new catalogs provide stellar masses with a better constrains for a subset of the complete sample SDSS+eBOSS.

Systematical biases and errors

It is well known that stellar population properties derived from data depend on the assumed models and modelling techniques, as routinely discussed in the literature. Here we focus on comparing stellar masses from this paper to previous releases, as this is the output that was previously provided. Bernardi et al. (2016) discuss in detail systematic uncertainties on stellar mass and stellar mass function, concluding that the dominant one is the assumed stellar population models. They showed that for the same IMF, different assumptions on the adopted stellar population models cause up to 0.3 dex systematic differences. Different dust models lead to 0.2 dex systematic differences. On top of these systematics, the assumed IMF gives an offset, which is e.g.. of the order 0.2 dex passing

Fig. 17. Comparison of the stellar masses obtained with its preceding catalog the ‘starforming’ flavour of the calculations by the Portsmouth group for the data release 12 (Maraston et al. 2013).



from a Chabrier or Kroupa IMF to a Salpeter one (e.g. Pforr et al. 2012). As discussed in several papers (Maraston et al. 2010; Pforr et al. 2012), even when the same stellar population model is assumed, different assumption in the star formation history templates reflect themselves in stellar mass offsets. All effects settle around a 0.3 dex systematics in most cases. Sometimes the choice is to average stellar mass determinations from different modelling approaches and use the average for mass function studies (as in Bundy et al. 2017).

Here we compare the catalogs presented here to the ‘starforming’ flavour of the calculations by the Portsmouth group for the data release 12 (Maraston et al. 2013) and available at http://www.sdss.org/dr14/spectro/galaxy_portsmouth, see Fig. 17. We choose this flavour as it includes fitting templates with low ages as in our current calculations⁶. The agreement between the SDSS stellar masses is excellent. A larger scatter is found in the comparison of BOSS galaxies’ stellar masses, which is captured by the uncertainties. We found the distribution normed by area of the quantity $|M_1 - M_2| / \sqrt{\sigma_{M_1}^2 + \sigma_{M_2}^2}$ where M_1 and M_2 are the DR12 and the DR14 versions of the stellar mass measurement to be very close to a normal distribution if using 2σ errors. If using 1σ errors, there is a some level of tension between the catalogs between the BOSS catalogs. However, when we consider the subset where galaxies have the same redshift (within 0.001) and the same $E(B - V)$ (within 0.02), then the tension at 1σ disappears. Overall, we conclude that the agreement with previous calculations - considering the different fitting methods and assumed templates (within the same stellar evolution framework) - is good. The question on whether stellar masses calculated via spectroscopy or spectrophotometry compare is an ongoing question (partly addressed in Maraston et al. 2013, Appendix), which we should.

Furthermore we find that the average uncertainties on stellar mass, age and metallicity are systematically larger when comparing the M11-ELODIE results to the M11-STELIB ones. We disproved that this may be due to the different wavelength coverage. Given the complexity of stellar library input, we are not able to pin down the exact reason and we leave this for future investigations.

Performance on the data

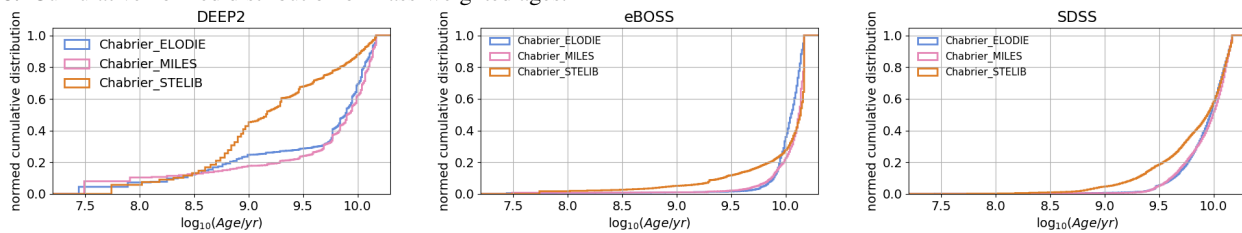
We follow the Lee et al. (2013) procedure to mask pixels affected by the sky and estimate the median SNR. The median SNR in all good pixels in the i -band of the spectrum is anticorrelated to the uncertainty. The higher the SNR, the smaller the uncertainty, see Fig. 16.⁷ This correlation holds up to redshift ~ 0.4 . Then the band of importance between 3500-5500Å break starts to enter the z -band where the estimation of the SNR are much noisier. So, at low redshift ($z < 0.3$), the selection of the best fits can be based on either the SNR or on the uncertainty on the stellar mass. At higher redshift ($z > 0.3$), the median SNR measure provided in the SDSS specObj summary files is not a reliable estimate of the actual SNR.

Trends in SDSS data: source type, signal to noise ratio, redshift

SDSS, BOSS and eBOSS have large numbers of programs (or sub components) that we split according to the ‘SOURCETYPE’ flag (there exist of order of ~ 200 different programs). Among these programs only eight contain more than 10,000 spectra classified as galaxies: GALAXY, NONLEGACY, QSO, QA in SDSS and LRG, QSO, SEQUELS_TARGET, SPIDERS_RASS_CLUS in eBOSS. Then in eBOSS of order of 40 programs have between 1,000 and 10,000 galaxy spectra. We give the number of galaxies split by SDSS (eBOSS) program in Table C.1 (C.2). (Note that the SOURCETYPE corresponds to the type it was assigned the first time it was targeted. To construct full sample, one needs to use target bits.) We give the number of galaxies considered for the fit and the fraction where the stellar mass parameter was constrained at better than 0.4 and 0.2 dex. In SDSS, the target type ‘GALAXY’ has a constrained stellar mass for more than 95% of its galaxy spectra which have a positive median signal to noise ratio. More than

⁶ See Maraston et al. 2013 for the ‘passive’ flavour and how it compares to the star forming set of calculations.

⁷ Chen et al. (2012) achieved a similar conclusion by comparing the stellar mass obtained via their PCA-based full spectral fitting and the one from broad-band SED fitting. The two estimates converge at a SNR around 25. See also discussion in Maraston et al. (2013), Appendix.

Fig. 18. Cumulative normed distribution of mass-weighted ages.


80% have an uncertainty on the stellar mass parameter lower than ± 0.2 dex. In eBOSS, the dominant galaxy type is LRG and 60% have an uncertainty on the stellar mass parameter lower than ± 0.2 dex.

The fraction of objects with well-constrained parameters have three main dependences: redshift, signal to noise ratio and fraction of the light observed in the fiber. For each program with more than 100 galaxy spectra we break down the statistics as a function of these parameters. The dependence on signal to noise ratio and redshift is shown in Table C.3 (C.4). It gives for five redshift bins (with boundaries 0, 0.025, 0.375, 0.7, 0.85, 1.6) the percentile of galaxies that corresponds to a median SNR of 5 or 20. For redshifts $z < 0.375$ more than half of the SDSS GALAXY (total $\sim 800,000$) have SNR greater than 20. For redshifts $z > 0.375$ not a single SDSS GALAXY (total $\sim 40,000$) has a SNR greater than 5. Low redshift galaxies ($z < 0.4$) were observed on average at higher signal to noise ratio than higher redshift galaxies. The panels of Fig. 16 show how the median signal to noise in good pixels in a band around the 4000Å break correlates with the uncertainty on the stellar mass (for 3 redshift bins, $0 < z < 0.02$, $0.02 < z < 0.38$ and $0.38 < z < 0.7$).

The dependence on the fraction of light observed and redshift is given in Table C.5 (C.6) It gives, in three redshift bins (with boundaries 0, 0.17, 0.55, 1.6), the number of galaxies where the fraction of the light in the fiber compared to the total light is greater than 50% (10%) i.e. the fiber magnitude smaller than the total magnitude by no more than 0.75 mag (2.5 mag). At redshift $z < 0.17$, most SDSS galaxies have between 10 and 50% of the light in the fiber, indeed their extension is larger than the fiber size. At high redshift $z > 0.55$, more than a third of the eBOSS LRG galaxies have more than 50% of their light in the fiber.

Common objects between SDSS, eBOSS and DEEP2

There are galaxies which were observed by both SDSS and DEEP2, precisely 64 (493) galaxies were observed by both DEEP2 and SDSS (eBOSS). Among these, 31 (261) have redshift values that agree within $|z_{DEEP2} - z_{SDSS(eBOSS)}| < 0.0005$. 3 (31) galaxies have a stellar mass constrained within ± 0.2 dex. For these 3+31 galaxies, the estimated stellar masses agree within errors.

Comparison with previous calculations

Compared to previous stellar population model catalogs, we roughly double the number of galaxies for which parameters were measured (DR12, Maraston et al. 2013; Thomas et al. 2013). In particular the number of well-constrained stellar masses (i.e. constrained to better than 0.2 dex at given IMF) has also doubled. Compared to previous studies of the SDSS data based on spectrophotometry (e.g. Maraston et al. 2013), the sample size of galaxies with parameters constrained to this level is increased by a factor of 2. Parameters based on broad-band SEDs on the other hand could be calculated for all data as they are less dependent on the SNR of the spectroscopic data. Hence, such a gain in precision is enabled by fitting every pixel of the spectra rather than only using the broad-band magnitudes (photometry) at the spectroscopic redshift. However, this is at the cost of having a less homogeneous sample. Indeed, the uncertainty on the stellar population parameters derived from full spectral fitting depends on the signal to noise ratio obtained in individual spectra, which varies according to observing conditions, position in the spectrograph and survey strategy. Hence, the tighter constrain on stellar parameters is gained at the price of completeness.

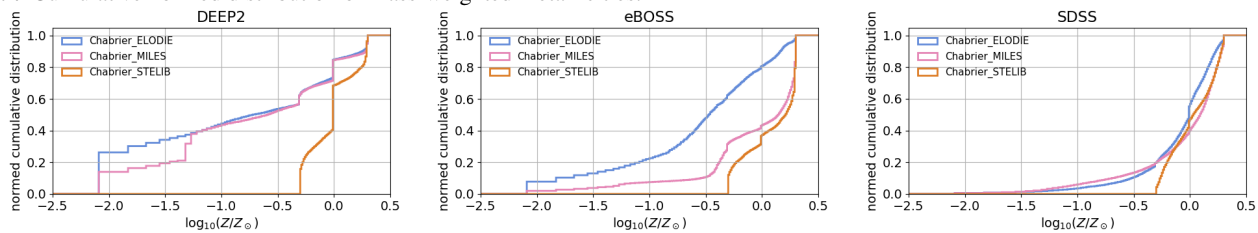
5.4. Ages, metallicities and star formation histories of galaxies

In this section we use our parameter estimates to construct a statistical view over the key population parameters, age, chemical composition and star formation history across our galaxy samples and across redshift. A more quantitative use of these results for a variety of galaxy evolution studies will be pursued in future investigations.

Galaxy ages

Fig. 18 shows the cumulative normed distribution of mass-weighted ages obtained for our three galaxy samples when using the three M11 model types (based on the ELODIE, MILES and STELIB), referred to a Chabrier IMF. We plot results for one IMF only as this parameter has little influence on the derived galaxy physical parameters (e.g. Pforr et al. 2012), when slope and exponents are not too different among the options.

Fitted mass-weighted ages obtained with M11-Miles and Elodie are remarkably consistent for the three galaxy samples, pointing to values larger than 3 Gyr, with over 60 % of the samples around 10 Gyr. Ages obtained with M11-Stelib models imply a $\sim 20\%$ of slightly younger galaxies due to their narrower coverage in metallicity and the age-metallicity degeneracy (by which the fit with

Fig. 19. Cumulative normed distribution of mass-weighted metallicities.

high metallicity models releases younger ages, e.g. Worthey 1994). Note also how nicely the age distribution for the DEEP2 sample containing higher-redshift galaxies selected to be star forming shifts to younger ages consistently for all models. Again here the effect at obtaining generally lower ages with M11-Stelib is even more pronounced, and 70% of the galaxies are younger than 3 Gyr.

Galaxy metallicity

Fig. 19 shows the cumulative normed distribution of mass-weighted metallicities fitted. There are some interesting trends to note. First of all, for the SDSS sample all models agree in pointing to high metallicities, with 80% of the sample having half-solar and above a chemical composition. The residual 20% is found to have lower metallicities by M11-MILES and M11-ELODIE as these contain low-metallicity models whereas M11-STELIB only span the range half-solar to twice solar (cfr. M11, Figure 3). Also for the DEEP2 sample (left-hand panel) M11-MILES and M11-ELODIE models give a very similar answer, with now 60% of the sample lying at subsolar metallicities. The M11-STELIB gives higher metallicities by construction, as already explained.

The eBOSS results are those revealing a larger scatter among the models, with M11-ELODIE giving a large fraction of metal-poor galaxies which is not found when fitting the other two models, which instead give the very similar result of high-metallicity also in the eBOSS galaxies.

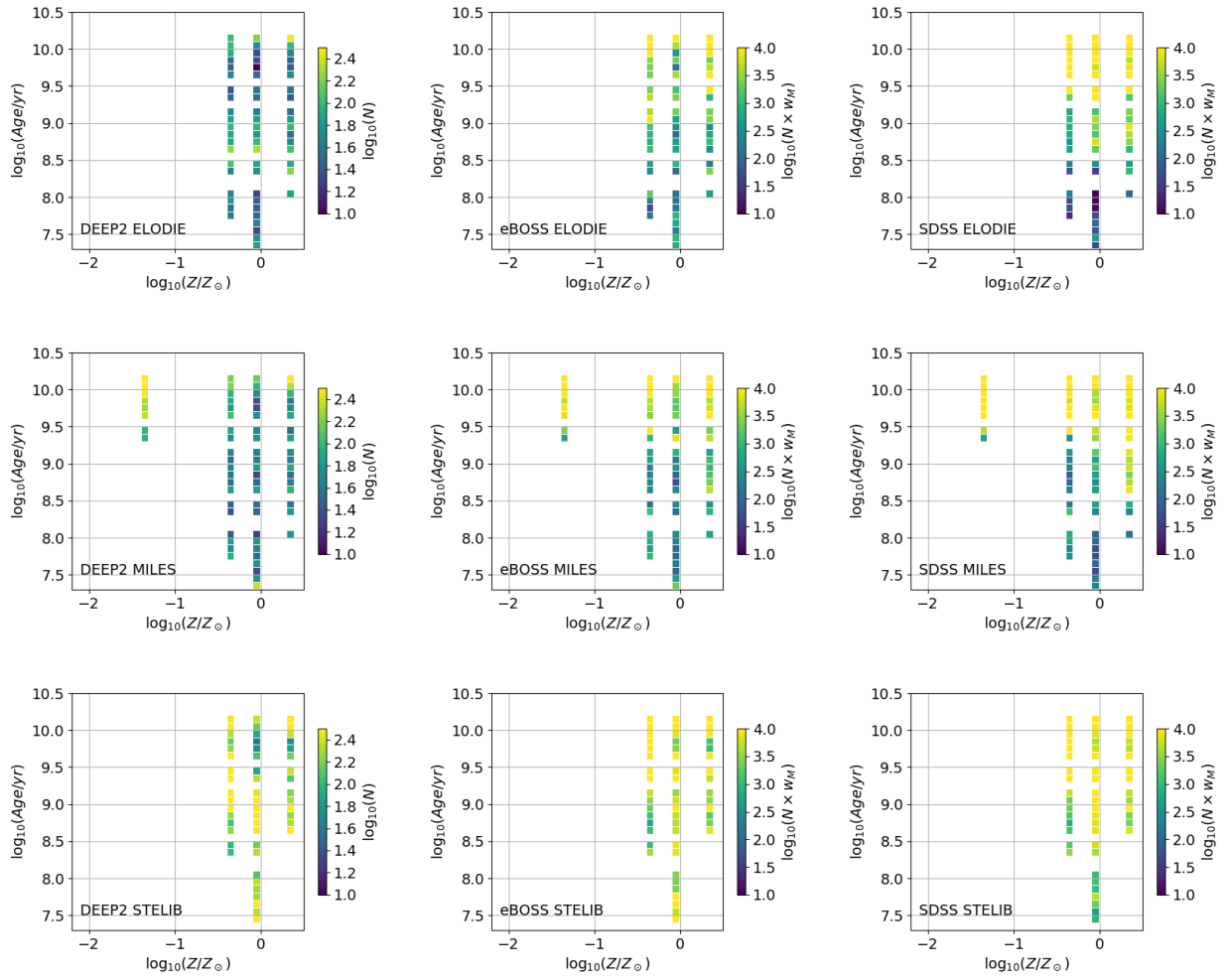
Galaxy star formation histories

Fig. 20 show the distribution of SSP components of the total best-fit to a galaxy, in the age-metallicity plane, colour-coded with the total number of components in a bin times the SSP weight. Those histograms have been obtained by adding the mass weights of all components in a small bin of age and metallicity. As in previous sections, plots refer to the M11-MILES, STELIB, ELODIE fitting models for a Chabrier IMF.

First of all, the fits with M11-MILES find a metal-poor old component in all galaxy samples. This could be interpreted as a metal-poor halo, which is known to exist in most galaxies. The weight of such a component is $\sim 15\%$ for SDSS and eBOSS and $\sim 45\%$ for DEEP2. The rest of the components for SDSS and eBOSS lie at higher metallicity, with the ages of the most metal-rich component spanning towards lower values, as expected by a gradual galaxy build-up where metal-enrichment proceeds with time. Obviously the details of individual objects will vary, for example massive ellipticals within the sample may show coeval, high metallicity populations, while massive spirals will be consistent with an age/metallicity relation of the kind just described. The same model on the DEEP2 sample gives less power to the high-metallicity components, and also a more homogenous age spread. This is reflecting the larger stellar age ranges found in this sample. M11-ELODIE give similar results for the high-metallicity components - a gradual decrease in age towards the highest metallicity - but does not reveal any low-metallicity part. Finally, M11-STELIB find all solutions at high-metallicity (larger than half solar by construction), but, differently from the other two models, present the largest fractions of lower ages (see yellow parts in the histograms), a fact that was already noted in M11 and Wilkinson et al. (2017).

These examples show how much the details of galaxy evolution are encapsulated in the interpretative model one assumes, although the macro characteristics of the galaxy components are - reassuringly - quite independent of the assumed model.

Fig. 20. Distribution of the SSP components in the age-metallicity plane color coded with the total number of components in a bin times the SSP mass weight (Chabrier IMF).



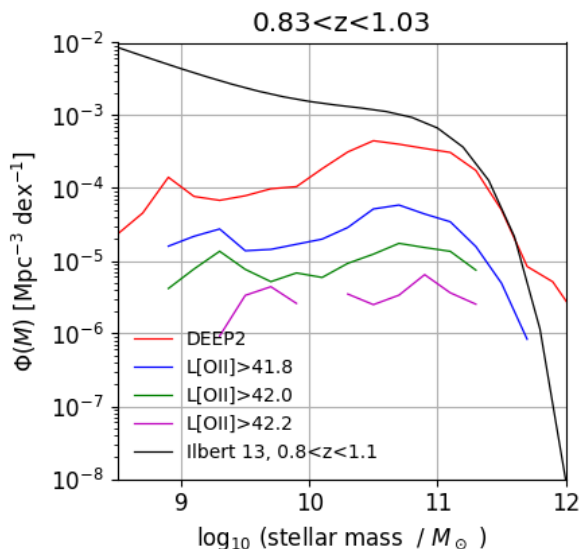


Fig. 21. Stellar mass function as measured in the DEEP2 [OII] emitter sample in the redshift range $0.83 < z < 1.03$ (considering all combinations of IMF and libraries). We show the stellar mass function is sampled by the [OII] emitters for different thresholds in $\log_{10}(L[\text{OII}])$ luminosity 41.8, 42 and 42.2.

6. Applications

6.1. Stellar mass function of galaxies selected with their [OII] emission line luminosity in DEEP2

How emission line galaxies populate the cosmic web is a hot topic in cosmology nowadays (Favole et al. 2016, 2017; Raichoor et al. 2017; Gonzalez-Perez et al. 2018; Guo et al. 2018). To characterize how emission line galaxies are related to the overall galaxy population, we project the DEEP2 observed stellar mass function in the redshift range $0.83 < z < 1.03$ for three [OII] luminosity threshold, $\log_{10}(L[\text{OII}]) > 41.8, 42$ and 42.2 , see Fig. 6.1. It is known that there is scatter in SFR at fixed mass and that the [OII]–SFR relation also has scatter. Therefore we do not expect to find that only a narrow range of masses is populated by the strongest [OII] emitters. Indeed, the distributions we find are quite broad, covering the stellar mass range $10^9 < M/M_{\odot} < 10^{11.5}$. More interestingly, these distributions are quite flat and their shape do not seem to depend on the luminosity threshold. Similar distributions are found in Raichoor et al. (2017); Guo et al. (2018). Given that the DEEP2 sample is complete for the [OII] luminosity limits applied, we conclude that up to $z = 1.5$ there is no preferred host galaxy mass (in the range $10^9 < M/M_{\odot} < 10^{11.5}$) to find a strong [OII] emission.

Recently, a broad range of properties of ELGs was predicted by the model presented in Gonzalez-Perez et al. (2018). In our data, it seems that massive galaxies are selected as [OII] emitters, where in the model, some of them are missing. This discrepancy is due to the treatment of the dust and to how emission lines are implemented in the model. A further detailed analysis is needed to understand better this very interesting puzzle.

The broad distribution in stellar mass underlying emission-line galaxies implies that stacked spectra of galaxies selected by emission line luminosity thresholds is unlikely to capture the variety of galaxies constituting the emission line galaxy population. The fact that any galaxy can be detected via emission-lines happens also because the light of emission-line selected galaxies is dominated by their latest generation of stars, which overshines the underlying structure of older stellar populations, much independently of the actual galaxy mass. This is (known as the ‘iceberg effect’ Maraston et al. 2010). A larger redshift range is needed to probe any dependence on mass of the ‘emission-line’ activity in galaxies.

6.2. Stellar mass function probed by SDSS, eBOSS and DEEP2

The galaxy stellar mass function and its evolution with redshift is a crucial probe of galaxy formation and evolution in a cosmological context (Bundy et al. 2006; Pozzetti et al. 2010; Maraston et al. 2013; Ilbert et al. 2013; Bernardi et al. 2016; Davidzon et al. 2017; Etherington et al. 2017). The study of this function requires large numbers of galaxies. For this reason usually the calculation of $\sim M^*$ is performed via broad-band photometry. It is therefore interesting to see what we obtain for the galaxy mass function when using our results based on spectral fitting rather than broad-band photometry, and for three different datasets in two redshift bins.

For eBOSS galaxies, we consider the area to be 10,000 deg², for SDSS 7,900 deg² and for DEEP2 0.5 deg² (low redshift) or 2.78 deg² (high redshift). For SDSS and eBOSS each galaxy represents itself only, no weighting other than the area is applied. It should be noted that Maraston et al. (2013) concluded that BOSS is complete down to $M \sim 10^{11} M_{\odot}$ (for a Kroupa IMF) up to $z \sim 0.55$ (see also Leauthaud et al. 2016, that reached a similar conclusion). The completeness of eBOSS has not yet been studied in depth. For DEEP2, we use the statistical weights from Comparat et al. (2016). These weights correct from the target selection algorithm used in DEEP2 and allow the recovery of the correct galaxy density as a function of redshift and magnitude.

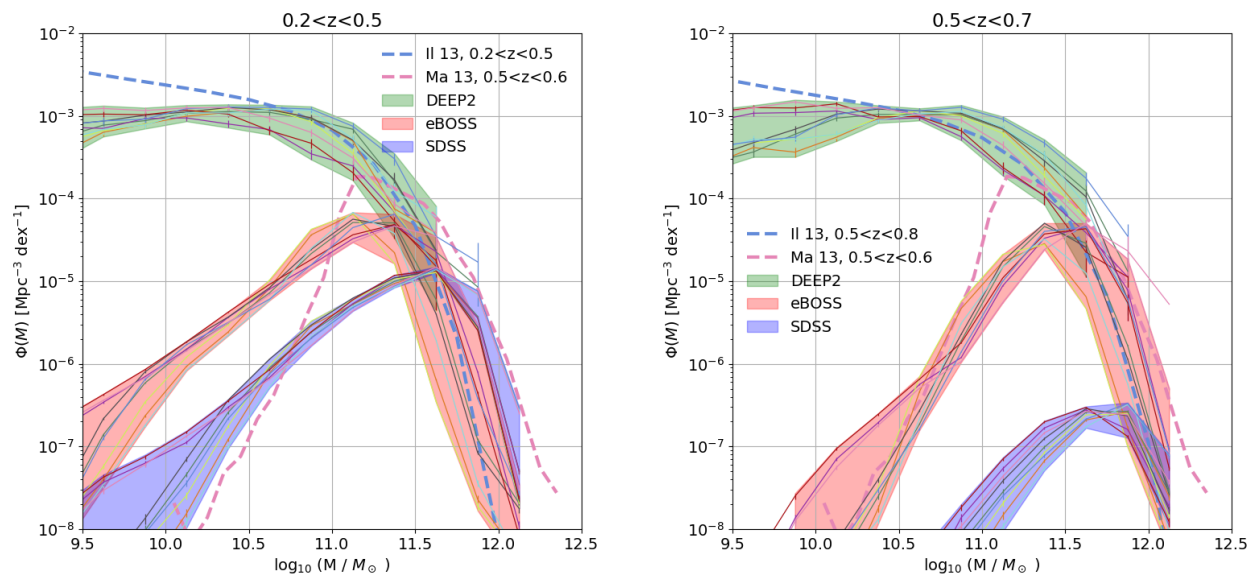


Fig. 22. Observed stellar mass function measured on SDSS, eBOSS and DEEP2 samples containing only well constrained stellar masses. Two redshift bins $0.2 < z < 0.5$, $0.5 < z < 0.7$ show how each survey spans the stellar mass function. For comparison, we added the Ilbert et al. (2013) model (green, they have the exact same redshift bins) and the BOSS SMF from Maraston et al. (2013), their mean measurement is at redshift 0.55 (magenta line).

For each catalog (3 surveys \times 3 libraries \times 3 IMF), we estimate the observed stellar mass function (OSMF) and its Poisson error (cosmic variance is not taken into account). We use only galaxies for which the stellar masses is constrained to better than 0.2 dex. Then, per each survey we compute the median of the nine measurements (i.e. over the three libraries \times three IMF) and the minimum and maximum of the nine measurements (with only Poisson errors considered). The OSMF obtained constitutes a robust a lower limit to the stellar mass function. Indeed because we use only stellar masses that are tightly constrained, we are certain that at least this density of stellar mass exists in galaxies.

We compare our results with the stellar mass functions obtained in COSMOS Ilbert et al. (2013) and in BOSS (Maraston et al. 2013). We show the results in two redshift bins: $0.2 < z < 0.5$, $0.5 < z < 0.8$, see Fig. 22. We see how each sample (DEEP2, SDSS, eBOSS), considering only the tightly constrained stellar masses, is related to the bulk of the galaxy population depicted by the COSMOS and BOSS stellar mass functions. This COSMOS stellar mass function is based on a K -band selected sample that is known to be biased at low redshift as it misses a fraction of the massive star-forming galaxy population i.e. at the high mass end our measurements are expected to be above that of COSMOS. This is what we find. The comparison with Maraston et al. (2013) (purple line on the Figure) shows the level of incompleteness we have due to our selection on the error on the stellar mass. Indeed we are incomplete as a function of magnitude and position on the sky. A detailed stellar mass function accounting for all selection function biases is left for future studies.

7. Summary and future releases

We provide the stellar population properties as obtained by full spectral fitting of models to the observed spectra for SDSS DR14 galaxies, including their high- z extensions (eBOSS), and for the DEEP2 survey mostly containing emission-line galaxies. We adopted the newly released FIREFLY fitting code coupled with the stellar population models by Maraston & Strömbäck (2011). This combination has improved the precision of derived parameters. In particular, the stellar mass for SDSS galaxies is obtained with a precision of about 0.2 dex for a given IMF, when $\text{SNR} > 20$. Thanks to the high performance computing environment "SCIAMA" at the University of Portsmouth, we could create models of the continuum for nine configurations of IMF and stellar libraries for about 2.7 million galaxies. This catalog is the continuation of the Portsmouth SDSS galaxy property catalogs, which were using the spectroscopic redshift combined with the broad-band photometry. Compared to previous releases, our work doubles the number of galaxies with a tightly constrained stellar mass parameter.

We explore for the first time stellar population modelling of DEEP2 emission line galaxies and find that these galaxies span a variety of properties, which is in broad agreement with predictions of the state-of-the-art semi-analytical models. In particular, DEEP2 galaxies selected by their [OII] luminosity in the redshift range $0.83 < z < 1.03$, have stellar masses with a constant number density in the range $10^9 < M(M_\odot) < 10^{11.5}$.

Ongoing FIREFLY developments expected for the next SDSS public release (DR16 onwards) are:

- Emission line measurements on the residuals.
- An AGN mode added to FIREFLY to allow for fitting all the pixels of AGN spectra (e.g. Calderone et al. 2017).

A variety of science cases will be explored in upcoming companion papers.

8. Acknowledgements

JC thanks the FIREFLY team for the team work and this milestone ! We all thank Gary Burton for his superb help and technical support with the SCIAMA machine, and Anne-Marie Weijmans for her guidance through the VAC emission.

VGP acknowledges support from the University of Portsmouth through the Dennis Sciama Fellowship award. Numerical computations were done on the SCIAMA High Performance Compute cluster which is supported by the ICG, SEPNet and the University of Portsmouth. This research used resources of the National Energy Research Scientific Computing Center, a DOE Office of Science User Facility supported by the Office of Science of the U.S. Department of Energy under Contract No. DE-AC02-05CH11231. This work has benefited from the publicly available programming language PYTHON.

Funding for the Sloan Digital Sky Survey IV has been provided by the Alfred P. Sloan Foundation, the U.S. Department of Energy Office of Science, and the Participating Institutions. SDSS acknowledges support and resources from the Center for High-Performance Computing at the University of Utah. The SDSS web site is www.sdss.org.

SDSS is managed by the Astrophysical Research Consortium for the Participating Institutions of the SDSS Collaboration including the Brazilian Participation Group, the Carnegie Institution for Science, Carnegie Mellon University, the Chilean Participation Group, the French Participation Group, Harvard-Smithsonian Center for Astrophysics, Instituto de Astrofísica de Canarias, The Johns Hopkins University, Kavli Institute for the Physics and Mathematics of the Universe (IPMU) / University of Tokyo, Lawrence Berkeley National Laboratory, Leibniz Institut für Astrophysik Potsdam (AIP), Max-Planck-Institut für Astronomie (MPIA Heidelberg), Max-Planck-Institut für Astrophysik (MPA Garching), Max-Planck-Institut für Extraterrestrische Physik (MPE), National Astronomical Observatories of China, New Mexico State University, New York University, University of Notre Dame, Observatório Nacional / MCTI, The Ohio State University, Pennsylvania State University, Shanghai Astronomical Observatory, United Kingdom Participation Group, Universidad Nacional Autónoma de México, University of Arizona, University of Colorado Boulder, University of Oxford, University of Portsmouth, University of Utah, University of Virginia, University of Washington, University of Wisconsin, Vanderbilt University, and Yale University.

References

- Abolfathi, B., Aguado, D. S., Aguilar, G., et al. 2017, ArXiv e-prints [arXiv:1707.09322]
 Beifiori, A., Maraston, C., Thomas, D., & Johansson, J. 2011, A&A, 531, A109
 Bernardi, M., Meert, A., Sheth, R. K., et al. 2016, MNRAS, 455, 4122
 Blanton, M. R., Bershady, M. A., Abolfathi, B., et al. 2017, AJ, 154, 28
 Bolton, A. S., Schlegel, D. J., Aubourg, É., et al. 2012, AJ, 144, 144
 Bruzual, G. & Charlot, S. 2003, MNRAS, 344, 1000
 Bundy, K., Ellis, R. S., Conselice, C. J., et al. 2006, ApJ, 651, 120
 Bundy, K., Leauthaud, A., Saito, S., et al. 2017, ApJ, 851, 34
 Calderone, G., Nicastro, L., Ghisellini, G., et al. 2017, MNRAS, 472, 4051
 Cappellari, M. & Emsellem, E. 2004, PASP, 116, 138
 Chabrier, G. 2003, PASP, 115, 763
 Chen, Y.-M., Kauffmann, G., Tremonti, C. A., et al. 2012, MNRAS, 421, 314
 Cid Fernandes, R., Mateus, A., Sodré, L., Stasińska, G., & Gomes, J. M. 2005, MNRAS, 358, 363
 Coil, A. L., Mendez, A. J., Eisenstein, D. J., & Moustakas, J. 2017, ApJ, 838, 87
 Comparat, J., Zhu, G., Gonzalez-Perez, V., et al. 2016, MNRAS, 461, 1076
 Conroy, C., Graves, G. J., & van Dokkum, P. G. 2014, ApJ, 780, 33
 Covington, M. D., Kassin, S. A., Dutton, A. A., et al. 2010, ApJ, 710, 279
 Davidzon, I., Ilbert, O., Laigle, C., et al. 2017, A&A, 605, A70
 Dawson, K. S., Kneib, J.-P., Percival, W. J., et al. 2016, AJ, 151, 44
 Etherington, J., Thomas, D., Maraston, C., et al. 2017, MNRAS, 466, 228

- Faber, S. M., Phillips, A. C., Kibrick, R. I., et al. 2003, in Society of Photo-Optical Instrumentation Engineers (SPIE) Conference Series, Vol. 4841, Instrument Design and Performance for Optical/Infrared Ground-based Telescopes, ed. M. Iye & A. F. M. Moorwood, 1657–1669
- Falcón-Barroso, J., Sánchez-Blázquez, P., Vazdekis, A., et al. 2011, *A&A*, 532, A95
- Favole, G., Comparat, J., Prada, F., et al. 2016, *MNRAS*, 461, 3421
- Favole, G., Rodríguez-Torres, S. A., Comparat, J., et al. 2017, *MNRAS*, 472, 550
- Goddard, D., Thomas, D., Maraston, C., et al. 2017a, *MNRAS*, 465, 688
- Goddard, D., Thomas, D., Maraston, C., et al. 2017b, *MNRAS*, 466, 4731
- Gonzalez-Perez, V., Comparat, J., Norberg, P., et al. 2018, *MNRAS*, 474, 4024
- Gunn, J. E., Siegmund, W. A., Mannery, E. J., et al. 2006, *AJ*, 131, 2332
- Guo, H., Yang, X., Raichoor, A., et al. 2018, arXiv e-prints, arXiv:1810.05318
- Ilbert, O., McCracken, H. J., Le Fèvre, O., et al. 2013, *A&A*, 556, A55
- Kassin, S. A., Weiner, B. J., Faber, S. M., et al. 2007, *ApJ*, 660, L35
- Kauffmann, G., Heckman, T. M., Tremonti, C., et al. 2003, *MNRAS*, 346, 1055
- Kroupa, P. 2001, *MNRAS*, 322, 231
- Le Borgne, J.-F., Bruzual, G., Pelló, R., et al. 2003, *A&A*, 402, 433
- Leauthaud, A., Bundy, K., Saito, S., et al. 2016, *MNRAS*, 457, 4021
- Lee, K.-G., Bailey, S., Bartsch, L. E., et al. 2013, *AJ*, 145, 69
- Lian, J., Thomas, D., Maraston, C., et al. 2018a, *MNRAS*, 474, 1143
- Lian, J., Thomas, D., Maraston, C., et al. 2018b, *MNRAS*, 476, 3883
- Maraston, C., Pforr, J., Henriques, B. M., et al. 2013, *MNRAS*, 435, 2764
- Maraston, C., Pforr, J., Renzini, A., et al. 2010, *MNRAS*, 407, 830
- Maraston, C. & Strömbäck, G. 2011, *MNRAS*, 418, 2785
- Mo, H., van den Bosch, F. C., & White, S. 2010, *Galaxy Formation and Evolution*
- Mostek, N., Coil, A. L., Cooper, M., et al. 2013, *ApJ*, 767, 89
- Newman, J. A., Cooper, M. C., Davis, M., et al. 2013, *ApJS*, 208, 5
- Parikh, T., Thomas, D., Maraston, C., et al. 2018, *MNRAS*, 477, 3954
- Pforr, J., Maraston, C., & Tonini, C. 2012, *MNRAS*, 422, 3285
- Planck Collaboration, Abergel, A., Ade, P. A. R., et al. 2014, *A&A*, 571, A11
- Pozzetti, L., Bolzonella, M., Zucca, E., et al. 2010, *A&A*, 523, A13
- Prugniel, P., Soubiran, C., Koleva, M., & Le Borgne, D. 2007, ArXiv Astrophysics e-prints [astro-ph/0703658]
- Raichoor, A., Comparat, J., Delubac, T., et al. 2017, *MNRAS*, 471, 3955
- Renzini, A. 2006, *ARA&A*, 44, 141
- Salpeter, E. E. 1955, *ApJ*, 121, 161
- Sánchez-Blázquez, P., Peletier, R. F., Jiménez-Vicente, J., et al. 2006, *MNRAS*, 371, 703
- Smee, S. A., Gunn, J. E., Uomoto, A., et al. 2013, *AJ*, 146, 32
- Thomas, D., Steele, O., Maraston, C., et al. 2013, *MNRAS*, 431, 1383
- Tojeiro, R., Wilkins, S., Heavens, A. F., Panter, B., & Jimenez, R. 2009, *ApJS*, 185, 1
- Tremonti, C. A., Heckman, T. M., Kauffmann, G., et al. 2004, *ApJ*, 613, 898
- Vazdekis, A., Koleva, M., Ricciardelli, E., Röck, B., & Falcón-Barroso, J. 2016, *MNRAS*, 463, 3409
- Wilkinson, D. M., Maraston, C., Goddard, D., Thomas, D., & Parikh, T. 2017, *MNRAS*, 472, 4297
- Wilkinson, D. M., Maraston, C., Thomas, D., et al. 2015, *MNRAS*, 449, 328

Table A.1. Data volume generated in this study.

Survey	catalog	spectra	models	total
SDSS	23G	278G	860G	1.1T
eBOSS	49G	0.5T	1.5T	2.1T
DEEP2	1.4G	6.2G	17G	24.6G

Appendix A: Description of the FIREFLY data

Appendix A.1: Processing

The processing was done on SCIAMA⁸, a high performance computing facility belonging to the University of Portsmouth (United Kingdom). A fit for a single model takes about a minute cpu so that the whole run required about 350,000 cpu hours. The total data volume is about 3.2T, as in Table A.1.

Appendix A.2: Public FIREFLY catalogs and data

For SDSS, all products are available here https://firefly.mpe.mpg.de/v1_1_0/26. For eBOSS, all products are available here https://firefly.mpe.mpg.de/v1_1_0/v5_10_0. A previous version of the SDSS/eBOSS firefly catalogs is available here https://data.sdss.org/sas/dr14/eboss/spectro/firefly/v1_0_4. For DEEP2, they are available here https://firefly.mpe.mpg.de/v1_1_0/DEEP2 (both versions). The data model is available at <http://www.sdss.org/dr14/spectro/eboss-firefly-value-added-catalog/>.

Model spectrum

The lowest level data product is the model file. There is one such file per galaxy spectrum considered. It is available for both DEEP2 and SDSS data sets. It is a fits file with a header and 9 data units. The primary header contains all input parameters used during the fit. The following nine data units each contain

- Header. The best fit parameters for each SSP entering the best model.
- Data extension. The best-fitting model spectrum: wavelength (Unit Angstrom) and model flux (f_λ convention, unit 10^{-17} erg $\text{cm}^{-2} \text{s}^{-1} \text{A}^{-1}$).

The nine data units contain the results obtained for the different combinations of stellar libraries and initial mass functions.

- HDU1 M11-MILES x Chabrier IMF
- HDU2 M11-MILES x Salpeter IMF
- HDU3 M11-MILES x Kroupa IMF
- HDU4 M11-ELODIE x Chabrier IMF
- HDU5 M11-ELODIE x Salpeter IMF
- HDU6 M11-ELODIE x Kroupa IMF
- HDU7 M11-STELIB x Chabrier IMF
- HDU8 M11-STELIB x Salpeter IMF
- HDU9 M11-STELIB x Kroupa IMF

The data model for this product, named 'spFly', is available here https://data.sdss.org/datamodel/files/EBOSS_FIREFLY/FIREFLY_VER/RUN2D/SPMODELS_VER/PLATE/spFly.html and the corresponding files here https://firefly.mpe.mpg.de/v1_1_0/26/stellarpop and here https://firefly.mpe.mpg.de/v1_1_0/v5_10_0/stellarpop. The DEEP2 result model spectra are provided here <http://www.mpe.mpg.de/~comparat/DEEP2/stellarpop/> and follow the naming convention 'spFly-deep2-MASK-OBJNUM.fits'. An automated summary plot is provided for each model file. It illustrates the spectrum, the models, and the fitted parameters, see Fig. 1, 2, 3.

Plate-level summary catalogs (SDSS only)

Due to the size of the SDSS data set and its structure, we create summary catalogs for each plate, named 'spFlyPlate'. They contain all output parameters from the fitting procedure. The data model for these catalogs is given here https://data.sdss.org/datamodel/files/EBOSS_FIREFLY/FIREFLY_VER/RUN2D/SPMODELS_VER/PLATE/spFlyPlate.html.

⁸ <http://www.sciama.icg.port.ac.uk/>

Table C.1. SDSS data sorted per source type. Ordered by decreasing number of galaxies (third column). The second column, 'N', gives the number of spectra labeled under this sourcetype. The third column, 'N galaxies', gives the number of spectra considered as galaxies and their fraction relatively to the second column. The fourth column, 'SNR ALL> 0', gives the number of spectra considered as galaxies with a positive median SNR over its spectrum. We consider this column as the reference sample to be fitted by FIREFLY, hence the '100%'. The fifth column, 'firefly constrained', gives the fraction of constrained fits and their fraction relative to the reference sample (column 4). For the 'GALAXY' sourcetype (first line), it is very high at 810540/829464 ~ 97.7%. The last two columns, ' $\sigma_{\log M} < 0.4$ ' (' $\sigma_{\log M} < 0.2$ '), give the fraction of fits that have a stellar mass constrained within 0.4 (0.2) dex. It is around 80% for the GALAXY and QA sourcetype.

sourcetype	N	N galaxies		SNR ALL> 0		firefly constrained		$\sigma_{\log M} < 0.4$		$\sigma_{\log M} < 0.2$	
	N	N	%	N	%	N	%	N	%	N	%
GALAXY	858244	829464	96	829464	100	810540	97	794149	95	673690	81
NONLEGACY	294745	75154	25	74899	100	68906	92	57586	76	33134	44
QSO	168563	22724	13	22724	100	19803	87	15252	67	8167	35
QA	20408	14608	71	14608	100	14286	97	13919	95	11630	79
SERENDIPITY_FIRST	7526	4163	55	4163	100	3953	95	3576	85	2249	54
ROSAT_D	7057	1704	24	1704	100	1642	96	1350	79	739	43
SERENDIPITY_DISTANT	4911	251	5	251	100	221	88	146	58	68	27
SERENDIPITY_BLUE	22871	70	0	70	100	54	77	31	44	12	17
STAR_WHITE_DWARF	2290	32	1	32	100	26	81	16	50	10	31
SERENDIPITY_MANUAL	68	27	39	27	100	25	92	20	74	14	51
STAR_CARBON	3458	22	0	22	100	20	90	15	68	9	40
REDDEN_STD	15363	13	0	13	100	11	84	10	76	8	61
STAR_BHB	14230	12	0	12	100	9	75	7	58	4	33
STAR_PN	14	8	57	8	100	6	75	0	0	0	0
SERENDIPITY_RED	2771	2	0	2	100	1	50	0	0	0	0
HOT_STD	3413	2	0	2	100	2	100	2	100	1	50
SPECTROPHOTO_STD	15366	1	0	1	100	1	100	1	100	1	100
STAR_BROWN_DWARF	560	1	0	1	100	0	0	0	0	0	0
STAR_CATY_VAR	6853	1	0	1	100	1	100	1	100	0	0
SKY	61967	0	0	0	100	0	0	0	0	0	0
STAR_SUB_DWARF	1226	0	0	0	100	0	0	0	0	0	0
STAR_RED_DWARF	14496	0	0	0	100	0	0	0	0	0	0

Summary catalogs

Top-level summary catalogs contain all of the fitted parameters. They are available here

- SDSS: https://firefly.mpe.mpg.de/v1_1_0/26/sdss_firefly-26.fits
- eBOSS: https://firefly.mpe.mpg.de/v1_1_0/v5_10_0/eboss_firefly-v5_10_0.fits
- DEEP2: https://firefly.mpe.mpg.de/v1_1_0/DEEP2/catalogs/zcat.deep2.dr4.v4.LFcatalogTC.Planck13.spm.v2.fits.gz

They can be download as follows

```
wget --no-check-certificate https://firefly.mpe.mpg.de/v1_1_0/26/sdss_firefly-26.fits .
```

The data model for the summary file for the eBOSS data is available at: https://data.sdss.org/datamodel/files/EBOSS_FIREFLY/FIREFLY_VER/RUN2D/eboss_firefly.html while the one for the SDSS data https://data.sdss.org/datamodel/files/EBOSS_FIREFLY/FIREFLY_VER/RUN2D/sdss_firefly.html. They differ by the redshift column: 'Z' for SDSS and 'Z_NOQSO' for eBOSS.

Assumptions in the IMF or templates induce systematic differences in the constrained parameters. Therefore, we do not provide a mean stellar mass based on these nine runs.

The SDSS and eBOSS summary files contain the columns described in Table C.8. The DEEP2 summary file columns are described in the readme on the website.

Appendix B: Warning about fits with unconstrained parameters

We would like to warn the future users about fits that led to unconstrained age, mass or metallicity parameters. Indeed for every spectrum, firefly provides an answer and the full pdf of each parameter. But sometimes, the pdf is so large that the uncertainties are as large as the parameters space itself. In such cases the value output should not be trusted.

Appendix C: Large tables

Table C.2. Same as Table C.1 for eBOSS.

source type	N		N galaxies		SNR ALL > 0		firefly constrained		$\sigma_{\log M} < 0.4$		$\sigma_{\log M} < 0.2$	
	N	N	N	%	N	%	N	%	N	%	N	%
LRG	1579529	1479496	93	906577	100	887235	97	769382	84	546392	60	
QSO	645501	116243	18	61892	100	43481	70	30035	48	12669	20	
SEQUELS_TARGET	100810	38871	38	38871	100	36251	93	26190	67	11253	28	
SPIDERS_RASS_CLUS	10623	10433	98	2573	100	2555	99	2530	98	2279	88	
WISE_COMPLETE	10019	9113	91	0	100	0	0	0	0	0	0	
HIZ_LRG	9541	7463	78	0	100	0	0	0	0	0	0	
RM_TILE1	11270	7342	65	7342	100	6351	86	5579	76	3075	41	
WISE_BOSS_QSO	15851	6664	42	4512	100	3732	82	3182	70	1957	43	
RM_TILE2	30331	6475	21	6475	100	4586	70	3391	52	1847	28	
BRIGHTGAL	5565	5361	96	3541	100	3403	96	3370	95	3292	93	
ELG_TEST1	7200	4525	62	0	100	0	0	0	0	0	0	
ELG1_EBOSS	4741	3616	76	0	100	0	0	0	0	0	0	
SN_GAL1	4042	3502	86	3496	100	3345	95	2797	80	1900	54	
ELG_DECALS_TEST1	5356	3423	63	0	100	0	0	0	0	0	0	
SEQUELS_ELG	4217	3059	72	3059	100	2763	90	1290	42	175	5	
BLUE_RADIO	2920	2874	98	1791	100	1744	97	1687	94	1390	77	
QSO_VAR_LF	9069	2507	27	2313	100	1888	81	1164	50	456	19	
QSO_WISE_FULL_SKY	8271	2482	30	1247	100	1037	83	856	68	408	32	
QSO_VAR_SDSS	22752	2297	10	1527	100	1205	78	855	56	339	22	
SEQUELS_ELG_LOWP	2982	2269	76	2269	100	2025	89	922	40	153	6	
FAINT_ELG	2699	2235	82	2235	100	1942	86	855	38	85	3	
QSO1_REOBS	16021	2153	13	443	100	242	54	142	32	41	9	
CLUSTER_MEMBER	2072	2056	99	577	100	568	98	565	97	521	90	
LRG_ROUND3	2486	2032	81	0	100	0	0	0	0	0	0	
GAL_NEAR_QSO	2037	1954	95	1140	100	1111	97	990	86	670	58	
TDSS_B	18880	1734	9	489	100	410	83	358	73	225	46	
ELG	3479	1650	47	409	100	348	85	153	37	25	6	
S82X_TILE1	2775	1608	57	0	100	0	0	0	0	0	0	
QSO_SUPPZ	4839	1512	31	1213	100	825	68	749	61	578	47	
STRIPE82BCG	1407	1388	98	1380	100	1359	98	1302	94	1122	81	
QSO_WISE_SUPP	3992	1065	26	1065	100	945	88	771	72	366	34	
SPIDERS_RASS_AGN	1378	1064	77	275	100	236	85	224	81	181	65	
XMM_PRIME	2444	1052	43	1052	100	911	86	761	72	447	42	
QSO_EBOSS_W3_ADM	4383	1044	23	1044	100	915	87	536	51	149	14	
TAU_STAR	1468	784	53	784	100	123	15	28	3	5	0	
ELAIS_N1_GMRT_TAYLOR	1032	766	74	766	100	731	95	550	71	313	40	
QSO_GRI	1963	696	35	503	100	406	80	303	60	148	29	
QSO_DEEP	3358	661	19	661	100	576	87	257	38	29	4	
QSO1_VAR_S82	5499	624	11	0	100	0	0	0	0	0	0	
S82X_TILE2	2621	624	23	0	100	0	0	0	0	0	0	
VARBAL	1077	616	57	399	100	283	70	270	67	223	55	
CHANDRAv1	1179	601	51	383	100	349	91	298	77	176	46	
XMMHR	731	575	78	360	100	346	96	304	84	217	60	
SPIDERS_XCLASS_CLUS	568	559	98	85	100	85	100	84	98	70	82	
FAINT_HIZ_LRG	685	543	79	543	100	525	96	369	68	120	22	
ELG_UGRIZW_TEST1	892	535	60	0	100	0	0	0	0	0	0	
ELG1_EXTENDED	659	500	75	0	100	0	0	0	0	0	0	
TEMPLATE_GAL_PHOTO	604	485	80	485	100	460	94	395	81	271	55	
XMMBRIGHT	622	461	74	317	100	292	92	254	80	187	59	
XMMRED	524	434	82	319	100	304	95	298	93	262	82	
QSO_AALs	680	379	55	249	100	162	65	156	62	132	53	
SN_LOC	416	373	89	372	100	355	95	295	79	213	57	
TDSS_FES_VARBAL	769	365	47	119	100	81	68	67	56	56	47	
25ORI_WISE_W3	484	349	72	349	100	325	93	317	90	264	75	
XMM_SECOND	669	332	49	332	100	305	91	254	76	163	49	
QSO_AAL	507	327	64	208	100	125	60	114	54	99	47	
CXORED	337	311	92	193	100	192	99	188	97	166	86	
TDSS_CP	1054	297	28	116	100	90	77	71	61	29	25	
BLAZXR	355	287	80	186	100	160	86	152	81	131	70	

Continued on next page

Table C.2. continued.

source type	N	N galaxies		SNR ALL > 0		firefly constrained		$\sigma_{\log M} < 0.4$		$\sigma_{\log M} < 0.2$	
	N	N	%	N	%	N	%	N	%	N	%
ELAIS_N1_LOFAR	413	285	69	285	100	273	95	227	79	162	56
KOEKAPbSTAR	542	282	52	282	100	1	0	1	0	0	0
ELAIS_N1_GMRT_GARN	367	280	76	280	100	266	95	223	79	154	55
QSO_VAR	1043	273	26	273	100	226	82	197	72	140	51
QSO_RIZ	1471	262	17	206	100	183	88	130	63	63	30
ELAIS_N1_FIRST	324	256	79	256	100	241	94	211	82	151	59
RADIO_2LOBE_QSO	1084	244	22	148	100	130	87	104	70	52	35
TEMPLATE_QSO_SDSS1	496	233	47	233	100	170	73	133	57	71	30
ELG_DES_TEST1	450	230	51	0	100	0	0	0	0	0	0
PTF_GAL	178	174	97	67	100	64	95	64	95	55	82
ELG_GRIW_TEST1	275	172	62	0	100	0	0	0	0	0	0
QSO_IAL	292	172	58	117	100	79	67	75	64	62	53
SPIDERS_PILOT	446	167	37	9	100	8	88	8	88	4	44
TDSS_FES_NQHISN	169	158	93	3	100	1	33	1	33	1	33
WHITEDWARF_SDSS	3898	157	4	112	100	46	41	36	32	27	24
25ORI_WISE	290	154	53	154	100	148	96	138	89	115	74
QSO_RADIO	239	148	61	96	100	69	71	68	70	57	59
CXOBRIGHT	169	145	85	104	100	90	86	83	79	63	60
TDSS_FES_DE	146	143	97	2	100	2	100	1	50	1	50
ELG_UGRIZWbright_TEST1	183	142	77	0	100	0	0	0	0	0	0
TDSS_FES_HYPQSO	352	138	39	4	100	3	75	1	25	0	0
SPIDERS_XMMSL_AGN	170	138	81	51	100	40	78	39	76	29	56
KOE2068_STAR	276	129	46	129	100	46	35	21	16	9	7
TDSS_PILOT	998	120	12	96	100	78	81	47	49	18	18
QSO_VAR_FPG	614	117	19	115	100	94	81	63	54	19	16
WHITEDWARF_NEW	4989	114	2	70	100	36	51	31	44	22	31
QSO_XD_KDE_PAIR	631	112	17	43	100	33	76	27	62	13	30
TEMPLATE_STAR_PHOTO	462	111	24	111	100	86	77	75	67	47	42
QSO_RADIO_AAL	150	110	73	78	100	53	67	50	64	44	56
DISKEMITTER_REPEAT	98	98	100	62	100	34	54	30	48	25	40
SN_GAL2	107	92	86	92	100	87	94	77	83	57	62
KOEKAP_STAR	302	80	26	80	100	12	15	5	6	3	3
BLAZGXR	136	79	58	50	100	44	88	40	80	35	70
KOE2023_STAR	234	64	27	64	100	23	35	9	14	5	7
VARs	134	52	38	52	100	39	75	34	65	21	40
QSO_RADIO_IAL	77	45	58	34	100	26	76	25	73	22	64
LBG	242	45	18	45	100	39	86	14	31	1	2
IAMASERS	48	43	89	11	100	11	100	11	100	11	100
RQSS_SF	103	35	34	35	100	33	94	17	48	2	5
BLAZGXQSO	51	35	68	19	100	11	57	11	57	9	47
ELAIS_N1_JVLA	58	34	58	34	100	31	91	22	64	13	38
TDSS_SPIDERS_PILOT	113	34	30	3	100	3	100	2	66	2	66
QSO_noAALs	66	33	50	16	100	12	75	12	75	10	62
XMMGRIZ	98	33	33	24	100	23	95	12	50	4	16
KQSO_BOSS	136	32	23	32	100	28	87	23	71	19	59
BLAZGRQSO	75	29	38	16	100	13	81	13	81	7	43
BLAZGRFLAT	71	27	38	21	100	19	90	17	81	17	81
STD	62522	25	0	19	100	10	52	10	52	7	36
SN_GAL3	25	23	92	23	100	22	95	21	91	16	69
KOE2023bSTAR	563	19	3	19	100	4	21	3	15	1	5
KOE2068bSTAR	602	17	2	17	100	4	23	4	23	1	5
CXOGRIZ	32	14	43	7	100	6	85	4	57	3	42
ODDBAL	21	13	61	8	100	6	75	6	75	2	25
TDSS_FES_MGII	24	12	50	0	100	0	0	0	0	0	0
OTBAL	12	11	91	8	100	7	87	7	87	4	50
XMMSDSS	15	10	66	0	100	0	0	0	0	0	0
RQSS_SFC	15	10	66	10	100	9	90	9	90	2	20
SEGUE1	2805	9	0	9	100	3	33	2	22	2	22
SDSSFILLER	2485	9	0	9	100	5	55	5	55	5	55

Continued on next page

Table C.2. continued.

source type	N	N galaxies		SNR ALL > 0		firefly constrained		$\sigma_{\log M} < 0.4$		$\sigma_{\log M} < 0.2$	
	N	N	%	N	%	N	%	N	%	N	%
TDSS_PILOT_SNHOST	8	7	87	7	100	7	100	6	85	5	71
BLAZGX	18	7	38	6	100	5	83	5	83	4	66
SEGUE2	1953	7	0	7	100	3	42	1	14	0	0
FBQSBAL	8	6	75	4	100	0	0	0	0	0	0
PREVBAL	25	5	20	5	100	3	60	2	40	0	0
BLAZR	6	4	66	4	100	4	100	4	100	3	75
fainterM	2806	4	0	4	100	3	75	1	25	0	0
QSO_HIZ	520	4	0	4	100	4	100	4	100	1	25
STD_WD	543	3	0	0	100	0	0	0	0	0	0
BLAZXRVAR	4	3	75	3	100	2	66	2	66	2	66
AMC	21	2	9	2	100	0	0	0	0	0	0
RED_KG	10457	2	0	2	100	1	50	1	50	1	50
SPEC_SN	2	2	100	2	100	2	100	2	100	2	100
HIZQSO82	64	2	3	2	100	2	100	1	50	0	0
LBQSBAL	6	1	16	1	100	0	0	0	0	0	0
LOW_MET	53	1	1	1	100	1	100	1	100	1	100
SPOKE	1229	1	0	1	100	0	0	0	0	0	0
TDSS_FES_HYPSTAR	208	1	0	0	100	0	0	0	0	0	0
S82X_TILE3	4	1	25	0	100	0	0	0	0	0	0
BLAZGVAR	2	1	50	1	100	1	100	0	0	0	0
TDSS_PILOT_PM	132	1	0	1	100	1	100	0	0	0	0
HIZQSOIR	121	1	0	0	100	0	0	0	0	0	0
HPM	75	1	1	1	100	0	0	0	0	0	0
fainterL	1276	1	0	0	100	0	0	0	0	0	0
brighterM	1787	0	0	0	100	0	0	0	0	0	0
TEMPLATE_STAR_SPECTRO	160	0	0	0	100	0	0	0	0	0	0
TDSS_FES_WDDM	54	0	0	0	100	0	0	0	0	0	0
TDSS_FES_DWARFC	96	0	0	0	100	0	0	0	0	0	0
brighterL	422	0	0	0	100	0	0	0	0	0	0
TDSS_FES_ACTSTAR	154	0	0	0	100	0	0	0	0	0	0
FLARE1	30	0	0	0	100	0	0	0	0	0	0
BLAZXRVAR	1	0	0	0	100	0	0	0	0	0	0
SPOKE2	95	0	0	0	100	0	0	0	0	0	0
CALSTAR	40	0	0	0	100	0	0	0	0	0	0
FLARE2	59	0	0	0	100	0	0	0	0	0	0
RVTEST	84	0	0	0	100	0	0	0	0	0	0
RQSS_STMC	2	0	0	0	100	0	0	0	0	0	0
RQSS_STM	6	0	0	0	100	0	0	0	0	0	0
QSO_STD	1776	0	0	0	100	0	0	0	0	0	0
NA	280513	0	0	0	100	0	0	0	0	0	0
MTEMP	75	0	0	0	100	0	0	0	0	0	0
GES	263	0	0	0	100	0	0	0	0	0	0

Table C.3. SDSS sourcetypes containing more than 100 galaxies (column 3 of the previous table). We divide the data in five redshift using the boundaries 0, 0.025, 0.375, 0.7, 0.85 and 1.6. In each bin, we show the percentiles corresponding to SNR 5 and 20 around $(1+z)4000 \text{ \AA}$. The percentages shown correspond to the fraction of the data in the redshift bin with a SNR lower than 5 (20). The lower the percentile the higher the fraction of higher SNR data. More than half of the spectra, with a sourcetype='GALAXY' and a redshift lower than 0.375, has a signal to noise ratio above 20. All the data at redshift higher than 0.375 has a median SNR lower than 5. '-1' means that data is not available.

programname	N galaxies	$0 < z < 0.025$			$0.025 < z < 0.375$		
		N	% ₅	% ₂₀	N	% ₅	% ₂₀
GALAXY	829464	24203	8	67	764226	4	48
NONLEGACY	74899	1826	35	72	62961	12	90
QSO	22724	1119	2	59	20524	3	85
QA	14608	358	7	67	13425	2	50
SERENDIPITY_FIRST	4163	1	100	100	1667	13	95
ROSAT_D	1704	17	19	78	1360	32	95
SERENDIPITY_DISTANT	251	1	100	100	247	96	100
programname	N galaxies	$0.375 < z < 0.7$			$0.7 < z < 0.85$		
		N	% ₅	% ₂₀	N	% ₅	% ₂₀
GALAXY	829464	40916	100	100	54	100	100
NONLEGACY	74899	9775	100	100	255	100	100
QSO	22724	886	100	100	135	100	100
QA	14608	814	100	100	6	100	100
SERENDIPITY_FIRST	4163	2377	100	100	88	100	100
ROSAT_D	1704	319	100	100	6	100	100
SERENDIPITY_DISTANT	251	2	100	100	0	-1	-1
programname	N galaxies	$0.85 < z < 1.6$					
		N	% ₅	% ₂₀			
GALAXY	829464	65	100	100			
NONLEGACY	74899	82	100	100			
QSO	22724	60	100	100			
QA	14608	5	100	100			
SERENDIPITY_FIRST	4163	30	100	100			
ROSAT_D	1704	2	100	100			
SERENDIPITY_DISTANT	251	1	100	100			

Table C.4. Same as Table C.3 for eBOSS spectra.

programname	N galaxies	$0 < z < 0.025$			$0.025 < z < 0.375$		
		N	% ₅	% ₂₀	N	% ₅	% ₂₀
LRG	906577	117	31	73	168026	4	71
QSO	61892	1652	35	95	35238	57	95
SEQUELS_TARGET	38871	533	44	95	9819	43	94
RM_TILE1	7342	3	81	100	2398	8	65
RM_TILE2	6475	410	13	89	4357	34	92
WISE_BOSS_QSO	4512	157	4	96	2257	4	95
BRIGHTGAL	3541	543	3	43	2996	0	4
SN_GAL1	3496	1	100	100	2474	28	87
SEQUELS_ELG	3059	2	100	100	624	90	100
SPIDERS_RASS_CLUS	2573	2	100	100	2230	4	65
QSO_VAR_LF	2313	98	27	82	1328	64	95
SEQUELS_ELG_LOWP	2269	3	100	100	556	93	99
FAINT_ELG	2235	1	100	100	14	59	100
BLUE_RADIO	1791	1	100	100	830	4	95
QSO_VAR_SDSS	1527	45	35	100	706	53	95
STRIPE82BCG	1380	0	-1	-1	895	3	73
QSO_WISE_FULL_SKY	1247	25	24	96	688	35	96
QSO_SUPPZ	1213	9	100	72	646	3	77
GAL_NEAR_QSO	1140	0	-1	-1	479	18	99
QSO_WISE_SUPP	1065	28	41	100	376	24	95
XMM_PRIME	1052	18	48	100	424	23	78
QSO_EBOSS_W3_ADM	1044	19	33	96	510	66	95
TAU_STAR	784	11	44	86	608	41	99
ELAIS_N1_GMRT_TAYLOR	766	0	-1	-1	372	20	90

Table C.4. continued.

QSO_DEEP	661	2	100	100	288	97	100			
CLUSTER_MEMBER	577	0	-1	-1	499	2	77			
FAINT_HIZ_LRG	543	0	-1	-1	1	100	100			
QSO_GRI	503	49	92	100	140	52	97			
TDSS_B	489	5	75	94	281	23	90			
TEMPLATE_GAL_PHOTO	485	5	25	100	307	14	77			
QSO1_REOBS	443	3	24	100	300	82	99			
ELG	409	16	75	100	128	94	100			
VARBAL	399	3	100	100	270	0	58			
CHANDRAv1	383	21	10	57	154	10	90			
SN_LOC	372	22	4	47	334	27	75			
XMMHR	360	0	-1	-1	186	4	91			
25ORI_WISE_W3	349	0	-1	-1	255	3	86			
XMM_SECOND	332	2	100	93	161	22	75			
XMMRED	319	0	-1	-1	237	2	89			
XMMBRIGHT	317	3	100	100	179	4	90			
ELAIS_N1_LOFAR	285	4	100	38	139	20	60			
KOEKAPbSTAR	282	0	-1	-1	0	-1	-1			
ELAIS_N1_GMRT_GARN	280	0	-1	-1	160	15	75			
SPIDERS_RASS_AGN	275	1	100	100	192	0	47			
QSO_VAR	273	12	100	70	164	5	90			
ELAIS_N1_FIRST	256	0	-1	-1	135	7	55			
QSO_AALs	249	6	100	100	130	100	4			
TEMPLATE_QSO_SDSS1	233	3	100	100	126	14	83			
QSO_AAL	208	1	100	100	112	100	100			
QSO_RIZ	206	5	8	44	64	66	99			
CXORED	193	1	100	100	153	100	93			
BLAZXR	186	1	100	100	119	3	70			
25ORI_WISE	154	0	-1	-1	98	4	90			
RADIO_2LOBE_QSO	148	2	100	100	54	38	100			
KOE2068_STAR	129	1	100	100	112	5	88			
TDSS_FES_VARBAL	119	1	100	100	92	4	90			
QSO_IAL	117	1	100	100	66	100	1			
TDSS_CP	116	0	-1	-1	51	27	100			
QSO_VAR_FPG	115	1	100	100	65	52	100			
WHITEDWARF_SDSS	112	10	100	33	40	100	54			
TEMPLATE_STAR_PHOTO	111	6	100	57	40	100	59			
CXOBRIGHT	104	1	100	100	53	100	82			
programname	N galaxies	0.375 < z < 0.7			0.7 < z < 0.85			0.85 < z < 1.6		
		N	% ₅	% ₂₀	N	% ₅	% ₂₀	N	% ₅	% ₂₀
LRG	906577	699627	95	100	36243	100	100	2564	100	100
QSO	61892	12247	95	100	8020	100	100	4735	100	100
SEQUELS_TARGET	38871	14835	95	98	9114	100	100	4570	100	100
RM_TILE1	7342	2144	93	100	1576	100	100	1221	100	100
RM_TILE2	6475	1359	95	99	271	100	100	78	100	100
WISE_BOSS_QSO	4512	1335	94	99	360	100	100	403	100	100
BRIGHTGAL	3541	2	100	100	0	-1	-1	0	-1	-1
SN_GAL1	3496	900	91	100	90	100	100	31	100	100
SEQUELS_ELG	3059	1594	100	100	444	100	100	395	100	100
SPIDERS_RASS_CLUS	2573	340	91	100	1	100	100	0	-1	-1
QSO_VAR_LF	2313	446	95	100	260	100	100	181	100	100
SEQUELS_ELG_LOWP	2269	1151	100	100	291	100	100	268	100	100
FAINT_ELG	2235	460	100	100	868	100	100	892	100	100
BLUE_RADIO	1791	942	80	100	14	100	100	4	100	100
QSO_VAR_SDSS	1527	371	95	100	241	100	100	164	100	100
STRIPE82BCG	1380	478	81	100	7	100	100	0	-1	-1
QSO_WISE_FULL_SKY	1247	220	96	100	193	100	100	121	100	100
QSO_SUPPZ	1213	413	82	98	132	100	100	13	100	100
GAL_NEAR_QSO	1140	645	92	100	15	100	100	1	100	100
QSO_WISE_SUPP	1065	432	95	100	147	100	100	82	100	100
XMM_PRIME	1052	390	95	99	143	100	100	77	100	100
QSO_EBOSS_W3_ADM	1044	341	96	100	107	100	100	67	100	100

Table C.4. continued.

TAU_STAR	784	44	100	100	11	100	100	110	100	100
ELAIS_N1_GMRT_TAYLOR	766	306	96	100	49	100	100	39	100	100
QSO_DEEP	661	162	100	100	123	100	100	86	100	100
CLUSTER_MEMBER	577	78	89	100	0	-1	-1	0	-1	-1
FAINT_HIZ_LRG	543	370	100	100	153	100	100	19	100	100
QSO_GRI	503	305	96	100	8	100	100	1	100	100
TDSS_B	489	107	90	98	34	100	100	62	100	100
TEMPLATE_GAL_PHOTO	485	166	96	100	5	100	100	2	100	100
QSO1_REOBS	443	90	100	100	4	100	100	46	100	100
ELG	409	96	100	100	80	100	100	89	100	100
VARBAL	399	91	77	100	28	100	100	7	100	100
CHANDRAv1	383	158	96	100	39	100	100	11	100	100
SN_LOC	372	13	97	100	3	100	100	0	-1	-1
XMMHR	360	151	93	100	16	100	100	7	100	100
25ORI_WISE_W3	349	88	99	100	2	100	100	4	100	100
XMM_SECOND	332	111	96	100	41	100	100	17	100	100
XMMRED	319	82	83	100	0	-1	-1	0	-1	-1
XMMBRIGHT	317	110	87	100	10	100	100	15	100	100
ELAIS_N1_LOFAR	285	96	93	100	30	100	100	16	100	100
KOEKAPbSTAR	282	274	100	100	8	100	100	0	-1	-1
ELAIS_N1_GMRT_GARN	280	88	94	100	15	100	100	17	100	100
SPIDERS_RASS_AGN	275	40	75	100	15	100	100	27	100	100
QSO_VAR	273	52	87	100	17	100	100	28	100	100
ELAIS_N1_FIRST	256	89	90	100	19	100	100	13	100	100
QSO_AALs	249	83	79	98	19	100	100	11	100	100
TEMPLATE_QSO_SDSS1	233	74	93	100	18	100	100	12	100	100
QSO_AAL	208	52	74	99	19	100	100	24	100	100
QSO_RIZ	206	78	97	100	55	100	100	4	100	100
CXORED	193	39	85	100	0	-1	-1	0	-1	-1
BLAZXR	186	44	80	100	15	100	100	7	100	100
25ORI_WISE	154	55	99	100	0	-1	-1	1	100	100
RADIO_2LOBE_QSO	148	45	95	100	29	100	100	18	100	100
KOE2068_STAR	129	5	46	100	4	100	100	7	100	100
TDSS_FES_VARBAL	119	14	94	100	4	100	100	8	100	100
QSO_IAL	117	35	51	96	4	100	100	11	100	100
TDSS_CP	116	25	96	100	14	100	100	26	100	100
QSO_VAR_FPG	115	20	100	100	11	100	100	18	100	100
WHITEDWARF_SDSS	112	45	67	96	11	100	100	6	100	100
TEMPLATE_STAR_PHOTO	111	32	90	100	22	100	100	11	100	100
CXOBRIGHT	104	36	88	100	4	100	100	10	100	100

Table C.5. SDSS source types containing more than 100 galaxies divided in three redshift to match the 4000Å break region to a SDSS broad band change to $g, r, i: 0 < z < 0.17, 0.17 < z < 0.55, 0.55 < z < 1.6$. This table is created only for objects with SDSS photometry. In each bin, we count the fraction of objects where the difference between fiber magnitude and model magnitude is smaller than 0.75 (2.5) i.e. where 50% (10%) or more of the galaxy light went in the fiber. The SDSS galaxies at low redshift are extended objects, so that most of them only have a small fraction of their light going in the fiber.

programname	N	z	0 < z < 0.17, g	mag > 50%	> 10%	z	0.17 < z < 0.55, r	mag > 50%	> 10%	z	0.55 < z < 1.6, i	mag > 50%	> 10%
GALAXY	829464	634828	627598	12823	585371	194198	192141	4646	191720	438	407	30	395
NONLEGACY	74899	35110	33981	6553	33257	38003	37445	10991	37405	1786	1723	918	1718
QSO	22724	15321	15028	4518	14753	7042	6891	4053	6887	361	351	347	350
QA	14608	10717	10584	285	9876	3869	3832	171	3822	22	21	11	20
SERENDIPITY_FIRST	4163	154	152	32	152	3240	3215	791	3215	769	759	333	759
ROSAT_D	1704	458	385	168	378	1188	1132	626	1130	58	54	27	54
SERENDIPITY_DISTANT	251	12	11	11	11	236	232	232	232	3	2	2	2

Table C.6. Same as Table C.5 for eBOSS sourcetypes.

programname	N	z	0 < z < 0.17, g	mag > 50%	> 10%	z	0.17 < z < 0.55, r	mag > 50%	> 10%	z	0.55 < z < 1.6, i	mag > 50%	> 10%
LRG	906577	21079	20411	1168	20147	557046	554121	146236	553802	328452	327943	118872	327548
QSO	61892	15656	13105	13032	13105	27561	26871	26795	26868	18675	18365	18321	18364
SEQUELS_TARGET	38871	3885	3091	2599	3087	12122	11553	9487	11552	22864	22678	13736	22677
RM_TILE1	7342	445	445	398	445	3279	3226	3035	3226	3618	3553	3460	3553
RM_TILE2	6475	2553	2530	2530	2530	3031	2995	2993	2995	891	885	880	885
WISE_BOSS_QSO	4512	1154	1151	1150	1151	2096	2085	2085	2085	1262	1261	1261	1261
BRIGHTGAL	3541	3534	3301	23	2388	7	3	0	2	0	0	0	0
SN_GAL1	3496	532	520	165	510	2661	2599	1611	2599	303	287	256	287
SEQUELS_ELG	3059	150	130	105	130	1358	1282	1096	1282	1551	1530	1271	1530
SPIEDERS_RASS_CLUS	2573	1076	1075	239	1063	1490	1484	936	1483	7	7	6	7
QSO_VAR_LF	2313	549	501	489	497	1146	1116	1105	1116	618	598	586	598
SEQUELS_ELG_LOWP	2269	120	111	83	111	1087	1050	899	1050	1062	1034	852	1033
FANT_ELG	2235	6	5	5	5	94	81	62	81	2135	1841	1405	1835
BLUE_RADIO	1791	6	5	3	5	1713	1709	677	1709	72	72	41	71
QSO_VAR_SDSS	1527	359	314	313	314	554	529	526	529	614	597	592	597
STRIPES2BCG	1380	164	161	35	158	1139	1116	497	1115	77	75	47	75
QSO_WISE_FULL_SKY	1247	292	287	287	287	549	547	545	547	406	406	406	406
QSO_SUPPZ	1213	365	365	365	365	450	450	450	450	398	398	398	398
GAL_NEAR_QSO	1140	2	2	1	2	1045	1027	517	1027	93	87	22	87
QSO_WISE_SUPP	1065	169	158	158	158	445	414	414	414	441	435	435	435
XMM_PRIME	1052	148	141	83	139	518	513	380	512	386	381	320	380
QSO_EBOSS_W3_ADM	1044	193	140	138	140	551	522	520	522	300	288	288	288
TAU_STAR	784	338	334	78	331	291	282	79	280	155	154	33	154
ELAIS_N1_GMRT_TAYLOR	766	84	82	18	82	504	495	264	495	178	171	127	171
QSO_DEEP	661	47	40	37	40	334	287	271	285	280	248	222	248

Continued on next page

Table C.6. continued.

CLUSTER_MEMBER	577	170	170	32	170	405	213	405	2	492	2	2	2
FAINT_HIZ_LRG	543	1	0	0	0	50	44	50	489	346	489	489	489
QSO_GRI	503	80	45	45	45	311	240	244	112	110	110	110	110
TDSS_B	489	58	55	53	55	305	242	289	126	125	126	126	126
TEMPLATE_GAL_PHOTO	485	201	201	57	200	225	127	224	59	29	58	58	58
QSO_REOBS	443	122	121	121	121	220	220	220	101	101	101	101	101
ELG	409	94	65	32	63	106	62	83	209	141	180	180	180
VARBAL	399	165	165	165	165	148	145	145	86	86	86	86	86
CHANDRAv1	383	62	46	34	44	235	175	213	86	66	74	74	74
SN_LOC	372	278	132	17	129	89	20	61	5	3	3	3	3
XMMHR	360	34	33	14	33	259	138	252	67	44	62	62	62
25ORI_WISE_W3	349	102	75	6	74	173	38	110	74	14	36	36	36
XMM_SECOND	332	44	44	8	42	180	97	175	108	77	107	107	107
XMMRED	319	34	33	10	33	274	99	266	11	5	8	8	8
XMMBRIGHT	317	32	31	23	31	227	153	217	58	53	57	57	57
ELAIS_N1_LOFAR	285	62	55	11	48	136	56	130	87	57	87	87	87
KOEKAPbSTAR	282	0	0	0	0	3	0	0	279	0	0	0	0
ELAIS_N1_GMRT_GARN	280	53	52	6	50	164	78	162	63	38	60	60	60
SPIBERS_RASS_AGN	275	73	72	23	72	153	98	152	49	43	49	49	49
QSO_VAR	273	110	95	93	95	99	88	88	64	58	58	58	58
ELAIS_N1_FIRST	256	49	48	4	48	133	40	130	74	41	74	74	74
QSO_AALs	249	69	69	69	69	103	103	103	77	76	76	76	76
TEMPLATE_QSO_SDSS1	233	33	33	33	33	140	138	140	60	60	60	60	60
QSO_AAL	208	36	36	36	36	108	108	108	64	64	64	64	64
QSO_RIZ	206	36	21	19	19	73	44	47	97	74	76	76	76
CXORED	193	28	26	11	26	160	62	157	5	1	3	3	3
BLAZXR	186	30	26	10	23	122	59	113	34	30	31	31	31
25ORI_WISE	154	27	19	1	18	77	14	52	50	17	31	31	31
RADIO_2LOBE_QSO	148	17	15	15	15	68	41	41	63	58	58	58	58
KOE2068_STAR	129	89	88	9	86	29	14	29	11	7	9	9	9
TDSS_FES_VARBAL	119	20	20	20	20	79	78	79	20	20	20	20	20
QSO_IAL	117	18	18	16	18	79	79	79	20	20	20	20	20
TDSS_CP	116	13	13	11	13	55	51	54	48	47	47	47	47
QSO_VAR_FPG	115	29	29	29	29	45	42	43	41	38	38	38	38
WHITEDWARF_SDSS	112	22	21	21	21	57	57	57	33	33	33	33	33
TEMPLATE_STAR_PHOTO	111	21	21	21	21	38	38	38	52	52	52	52	52
CXOBRIGHT	104	12	11	5	11	69	48	68	23	22	23	23	23

Table C.7. Same as Table C.5 for eBOSS sourcetypes.

programname	N	$0 < z < 0.17$, g			
		z	mag	> 10%	> 1%
LRG	906577	21079	20411	464	1259
QSO	61892	15656	13105	11238	13044
SEQUELS_TARGET	38871	3885	3091	1833	2648
RM_TILE1	7342	445	445	282	445
RM_TILE2	6475	2553	2530	2327	2530
WISE_BOSS_QSO	4512	1154	1151	1069	1151
BRIGHTGAL	3541	3534	3301	10	28
SN_GAL1	3496	532	520	33	190
SEQUELS_ELG	3059	150	130	55	107
SPIDERS_RASS_CLUS	2573	1076	1075	7	296
QSO_VAR_LF	2313	549	501	396	489
SEQUELS_ELG_LOWP	2269	120	111	36	87
FAINT_ELG	2235	6	5	3	5
BLUE_RADIO	1791	6	5	0	4
QSO_VAR_SDSS	1527	359	314	274	314
STRIPE82BCG	1380	164	161	5	41
QSO_WISE_FULL_SKY	1247	292	287	253	287
QSO_SUPPZ	1213	365	365	356	365
GAL_NEAR_QSO	1140	2	2	0	1
QSO_WISE_SUPP	1065	169	158	148	158
XMM_PRIME	1052	148	141	71	87
QSO_EBOSS_W3_ADM	1044	193	140	112	138
TAU_STAR	784	338	334	20	89
ELAIS_N1_GMRT_TAYLOR	766	84	82	3	21
QSO_DEEP	661	47	40	22	37
CLUSTER_MEMBER	577	170	170	1	44
FAINT_HIZ_LRG	543	1	0	0	0
QSO_GRI	503	80	45	30	45
TDSS_B	489	58	55	33	53
TEMPLATE_GAL_PHOTO	485	201	201	3	73
QSO1_REOBS	443	122	121	99	121
ELG	409	94	65	14	39
VARBAL	399	165	165	161	165
CHANDRAv1	383	62	46	30	37
SN_LOC	372	278	132	0	19
XMMHR	360	34	33	3	18
25ORI_WISE_W3	349	102	75	3	9
XMM_SECOND	332	44	44	5	9
XMMRED	319	34	33	1	12
XMMBRIGHT	317	32	31	16	25
ELAIS_N1_LOFAR	285	62	55	3	11
KOEKAPbSTAR	282	0	0	0	0
ELAIS_N1_GMRT_GARN	280	53	52	2	7
SPIDERS_RASS_AGN	275	73	72	4	24
QSO_VAR	273	110	95	72	93
ELAIS_N1_FIRST	256	49	48	3	5
QSO_AALs	249	69	69	67	69
TEMPLATE_QSO_SDSS1	233	33	33	33	33
QSO_AAL	208	36	36	33	36
QSO_RIZ	206	36	21	14	19
CXORED	193	28	26	2	11
BLAZXR	186	30	26	3	11
25ORI_WISE	154	27	19	1	2
RADIO_2LOBE_QSO	148	17	15	14	15
KOE2068_STAR	129	89	88	4	12
TDSS_FES_VARBAL	119	20	20	19	20
QSO_IAL	117	18	18	16	16
TDSS_CP	116	13	13	8	11

Continued on next page

Table C.7. continued.

QSO_VAR_FPG	115	29	29	27	29				
WHITEDWARF_SDSS	112	22	21	20	21				
TEMPLATE_STAR_PHOTO	111	21	21	21	21				
CXOBRIGHT	104	12	11	3	5				
programname	N	0.17 < z < 0.55, r				0.55 < z < 1.6, i			
		z	mag	> 10%	> 1%	z	mag	> 10%	> 1%
LRG	906577	557046	554121	7783	184634	328452	327943	9200	141815
QSO	61892	27561	26871	22589	26814	18675	18365	14854	18329
SEQUELS_TARGET	38871	12122	11553	3964	9945	22864	22678	3771	15167
RM_TILE1	7342	3279	3226	1762	3035	3618	3553	2219	3460
RM_TILE2	6475	3031	2995	2628	2993	891	885	752	883
WISE_BOSS_QSO	4512	2096	2085	1702	2085	1262	1261	1079	1261
BRIGHTGAL	3541	7	3	0	0	0	0	0	0
SN_GAL1	3496	2661	2599	233	1762	303	287	149	259
SEQUELS_ELG	3059	1358	1282	357	1144	1551	1530	391	1331
SPIDERS_RASS_CLUS	2573	1490	1484	69	1033	7	7	1	7
QSO_VAR_LF	2313	1146	1116	751	1108	618	598	502	590
SEQUELS_ELG_LOWP	2269	1087	1050	272	935	1062	1034	279	888
FAINT_ELG	2235	94	81	16	71	2135	1841	479	1479
BLUE_RADIO	1791	1713	1709	41	828	72	72	18	45
QSO_VAR_SDSS	1527	554	529	422	527	614	597	478	592
STRIPE82BCG	1380	1139	1116	61	577	77	75	11	54
QSO_WISE_FULL_SKY	1247	549	547	414	545	406	406	337	406
QSO_SUPPZ	1213	450	450	438	450	398	398	377	398
GAL_NEAR_QSO	1140	1045	1027	41	603	93	87	8	27
QSO_WISE_SUPP	1065	455	414	339	414	441	435	353	435
XMM_PRIME	1052	518	513	155	398	386	381	171	328
QSO_EBOSS_W3_ADM	1044	551	522	361	520	300	288	213	288
TAU_STAR	784	291	282	10	98	155	154	8	40
ELAIS_N1_GMRT_TAYLOR	766	504	495	35	293	178	171	41	138
QSO_DEEP	661	334	287	128	275	280	248	132	225
CLUSTER_MEMBER	577	405	405	6	248	2	2	0	2
FAINT_HIZ_LRG	543	50	50	5	47	492	489	45	380
QSO_GRI	503	311	249	177	241	112	110	77	110
TDSS_B	489	305	289	111	249	126	126	100	126
TEMPLATE_GAL_PHOTO	485	225	224	2	132	59	58	18	29
QSO1_REOBS	443	220	220	167	220	101	101	60	101
ELG	409	106	86	18	67	209	180	59	143
VARBAL	399	148	145	142	145	86	86	84	86
CHANDRAv1	383	235	214	58	182	86	74	44	66
SN_LOC	372	89	61	3	22	5	3	2	3
XMMHR	360	259	253	20	152	67	62	16	48
25ORI_WISE_W3	349	173	110	9	45	74	37	8	14
XMM_SECOND	332	180	175	22	101	108	107	27	79
XMMRED	319	274	266	6	123	11	8	1	5
XMMBRIGHT	317	227	217	58	161	58	57	38	53
ELAIS_N1_LOFAR	285	136	130	13	60	87	87	22	59
KOEKAPbSTAR	282	3	0	0	0	279	0	0	0
ELAIS_N1_GMRT_GARN	280	164	162	13	86	63	60	13	40
SPIDERS_RASS_AGN	275	153	152	21	103	49	49	33	44
QSO_VAR	273	99	88	76	88	64	58	55	58
ELAIS_N1_FIRST	256	133	130	8	52	74	74	10	45
QSO_AALs	249	103	103	100	103	77	76	69	76
TEMPLATE_QSO_SDSS1	233	140	140	133	138	60	60	58	60
QSO_AAL	208	108	108	105	108	64	64	62	64
QSO_RIZ	206	73	52	31	45	97	79	42	74
CXORED	193	160	157	2	74	5	3	1	1
BLAZXR	186	122	113	19	65	34	31	26	30
25ORI_WISE	154	77	52	2	16	50	31	5	17
RADIO_2LOBE_QSO	148	68	41	31	41	63	58	45	58
KOE2068_STAR	129	29	29	3	14	11	9	7	7

Continued on next page

Table C.7. continued.

TDSS_FES_VARBAL	119	79	79	72	78	20	20	19	20
QSO_IAL	117	79	79	76	79	20	20	19	20
TDSS_CP	116	55	54	38	51	48	47	41	47
QSO_VAR_FPG	115	45	43	37	42	41	38	30	38
WHITEDWARF_SDSS	112	57	57	54	57	33	33	31	33
TEMPLATE_STAR_PHOTO	111	38	38	38	38	52	52	52	52
CXOBRIGHT	104	69	68	10	51	23	23	17	23

Table C.8. Data model of the summary files. $\{\text{IMF}\}$ takes values in 'Chabrier', 'Kroupa', 'Salpeter'; $\{\text{LIBRARY}\}$ takes values in 'MILES', 'STELIB', 'ELODIE' and $\{i\}$ takes values in 0 to 9.

columns from Spec Obj All	FIREFLY columns	
SURVEY:	PLUG_RA:	
INSTRUMENT:	PLUG_DEC:	
CHUNK:	CLASS:	
PROGRAMNAME:	SUBCLASS:	$\{\text{IMF}\}_{\{\text{LIBRARY}\}}_{\text{age_lightW}}$: light weighted age in years
PLATERUN:	Z:	$\{\text{IMF}\}_{\{\text{LIBRARY}\}}_{\text{age_lightW_up_1sig}}$:
PLATEQUALITY:	Z_ERR:	$\{\text{IMF}\}_{\{\text{LIBRARY}\}}_{\text{age_lightW_low_1sig}}$:
PLATESN2:	RCHI2:	$\{\text{IMF}\}_{\{\text{LIBRARY}\}}_{\text{age_lightW_up_2sig}}$:
DEREDSN2:	DOF:	$\{\text{IMF}\}_{\{\text{LIBRARY}\}}_{\text{age_lightW_low_2sig}}$: errors
LAMBDA_EFF:	RCHI2DIFF:	$\{\text{IMF}\}_{\{\text{LIBRARY}\}}_{\text{metallicity_lightW}}$: light weighted metallicity in solar metallicity
BLUEFIBER:	TFILE:	
ZOFFSET:	TCOLUMN:	$\{\text{IMF}\}_{\{\text{LIBRARY}\}}_{\text{metallicity_lightW_up_1sig}}$:
SNTURNOFF:	NPOLY:	$\{\text{IMF}\}_{\{\text{LIBRARY}\}}_{\text{metallicity_lightW_low_1sig}}$:
NTURNOFF:	THETA:	$\{\text{IMF}\}_{\{\text{LIBRARY}\}}_{\text{metallicity_lightW_up_2sig}}$:
SPECPRIMARY:	VDISP:	$\{\text{IMF}\}_{\{\text{LIBRARY}\}}_{\text{metallicity_lightW_low_2sig}}$: errors
SPECSDSS:	VDISP_ERR:	$\{\text{IMF}\}_{\{\text{LIBRARY}\}}_{\text{age_massW}}$: mass weighted age in years
SPECLEGACY:	VDISPZ:	$\{\text{IMF}\}_{\{\text{LIBRARY}\}}_{\text{age_massW_up_1sig}}$:
SPECSEGUE:	VDISPZ_ERR:	$\{\text{IMF}\}_{\{\text{LIBRARY}\}}_{\text{age_massW_low_1sig}}$:
SPECSEGUE1:	VDISPCHI2:	$\{\text{IMF}\}_{\{\text{LIBRARY}\}}_{\text{age_massW_up_2sig}}$:
SPECSEGUE2:	VDISNPPIX:	$\{\text{IMF}\}_{\{\text{LIBRARY}\}}_{\text{age_massW_low_2sig}}$: errors
SPECBOSS:	VDISPDOF:	$\{\text{IMF}\}_{\{\text{LIBRARY}\}}_{\text{metallicity_massW}}$: mass weighted metallicity in solar metallicity
BOSS_SPECOBJ_ID:	WAVEMIN:	
SPECOBJID:	WAVEMAX:	$\{\text{IMF}\}_{\{\text{LIBRARY}\}}_{\text{metallicity_massW_up_1sig}}$:
FLUXOBJID:	WCOVERAGE:	$\{\text{IMF}\}_{\{\text{LIBRARY}\}}_{\text{metallicity_massW_low_1sig}}$:
BESTOBJID:	ZWARNING:	$\{\text{IMF}\}_{\{\text{LIBRARY}\}}_{\text{metallicity_massW_up_2sig}}$:
TARGETOBJID:	SN_MEDIAN_ALL:	$\{\text{IMF}\}_{\{\text{LIBRARY}\}}_{\text{metallicity_massW_low_2sig}}$: errors
PLATEID:	SN_MEDIAN:	$\{\text{IMF}\}_{\{\text{LIBRARY}\}}_{\text{stellar_mass}}$: total stellar mass in living stars + remnants + gas in solar mass
NSPECOBS:	CHI68P:	
FIRSTRELEASE:	FRACNSIGMA:	$\{\text{IMF}\}_{\{\text{LIBRARY}\}}_{\text{stellar_mass_up_1sig}}$:
RUN2D:	FRACNSIGHI:	$\{\text{IMF}\}_{\{\text{LIBRARY}\}}_{\text{stellar_mass_low_1sig}}$:
RUNID:	FRACNSIGLO:	$\{\text{IMF}\}_{\{\text{LIBRARY}\}}_{\text{stellar_mass_up_2sig}}$:
DESIGNID:	SPECTROFLUX:	$\{\text{IMF}\}_{\{\text{LIBRARY}\}}_{\text{stellar_mass_low_2sig}}$: errors
CX: CY: CZ:	SPECTROFLUX_IVAR:	$\{\text{IMF}\}_{\{\text{LIBRARY}\}}_{\text{living_star_mass}}$: stellar mass in living stars + remnants in solar mass
XFOCAL:	SPECTROSYNFLUX:	
YFOCAL:	SPECTROSYNFLUX_IVAR:	$\{\text{IMF}\}_{\{\text{LIBRARY}\}}_{\text{remnant_mass}}$: stellar mass in remnants
SOURCETYPE:	SPECTROSKYFLUX:	$\{\text{IMF}\}_{\{\text{LIBRARY}\}}_{\text{remnant_mass_in_whitedwarfs}}$: stellar mass in white dwarfs in solar mass
TARGETTYPE:	ANYANDMASK:	
THING_ID_TARGETING:	ANYORMASK:	$\{\text{IMF}\}_{\{\text{LIBRARY}\}}_{\text{remnant_mass_in_neutronstars}}$: stellar mass in neutron stars in solar mass
THING_ID:	SPEC1_G: SPEC1_R:	
PRIMTARGET:	SPEC1_I:	$\{\text{IMF}\}_{\{\text{LIBRARY}\}}_{\text{remnant_mass_blackholes}}$: stellar mass in black holes in solar mass
SECTARGET:	SPEC2_G: SPEC2_R:	
LEGACY_TARGET1:	SPEC2_I:	$\{\text{IMF}\}_{\{\text{LIBRARY}\}}_{\text{mass_of_ejecta}}$: stellar mass ejected in solar mass
LEGACY_TARGET2:	ELODIE_FILENAME:	$\{\text{IMF}\}_{\{\text{LIBRARY}\}}_{\text{spm_EBV}}$: reddening value fitted
SPECIAL_TARGET1:	ELODIE_OBJECT:	$\{\text{IMF}\}_{\{\text{LIBRARY}\}}_{\text{nComponentsSSP}}$: number of single stellar population components
SPECIAL_TARGET2:	ELODIE_SPTYPE:	
SEGUE1_TARGET1:	ELODIE_BV:	$\{\text{IMF}\}_{\{\text{LIBRARY}\}}_{\text{stellar_mass_ssp}_{\{i\}}}$: Stellar mass in the ith SSP
SEGUE1_TARGET2:	ELODIE_TEFF:	$\{\text{IMF}\}_{\{\text{LIBRARY}\}}_{\text{age_ssp}_{\{i\}}}$: Age of the ith SSP
SEGUE2_TARGET1:	ELODIE_LOGG:	$\{\text{IMF}\}_{\{\text{LIBRARY}\}}_{\text{metal_ssp}_{\{i\}}}$: Metallicity of the ith SSP
SEGUE2_TARGET2:	ELODIE_FEH:	$\{\text{IMF}\}_{\{\text{LIBRARY}\}}_{\text{weightMass_ssp}_{\{i\}}}$: mass weight of the ith SSP in the overall solution
MARVELS_TARGET1:	ELODIE_Z:	
MARVELS_TARGET2:	ELODIE_Z_ERR:	$\{\text{IMF}\}_{\{\text{LIBRARY}\}}_{\text{weightLight_ssp}_{\{i\}}}$: light weight of the ith SSP in the overall solution
BOSS_TARGET1:	ELODIE_Z_MODELERR:	
BOSS_TARGET2:	ELODIE_RCHI2:	$\{\text{IMF}\}_{\{\text{LIBRARY}\}}_{\text{chi2}}$: chi square
EBOSS_TARGET0:	ELODIE_DOF:	$\{\text{IMF}\}_{\{\text{LIBRARY}\}}_{\text{ndof}}$: Number of degree of freedom
EBOSS_TARGET1:	Z_NOQSO:	abs_mag_u_spec: abs_mag_g_spec: abs_mag_r_spec: abs_mag_i_spec:
EBOSS_TARGET2:	Z_ERR_NOQSO:	Absolute magnitude (u,g,r,i-band) measured on the observed spectrum
EBOSS_TARGET_ID:	ZWARNING_NOQSO:	abs_mag_u_noise: abs_mag_g_noise: abs_mag_r_noise: abs_mag_i_noise:
ANCILLARY_TARGET1:	CLASS_NOQSO:	Absolute magnitude (u,g,r,i-band) measured on the observed noise spectrum
ANCILLARY_TARGET2:	SUBCLASS_NOQSO:	SNR_ALL: Median signal to noise in the spectrum
SPECTROGRAPHID:	RCHI2DIFF_NOQSO:	SNR_32_35: Median signal to noise ratio in the band 3200-3500Å;
PLATE:	Z_PERSON:	SNR_35_39: - 3500-3900Å; SNR_39_41: - 3900-4100Å; SNR_41_55: -
TILE:	CLASS_PERSON:	4100-5500Å; SNR_55_68: - 5500-6800Å; SNR_68_74: - 6800-7400Å;
MJD:	Z_CONF_PERSON:	SNR_74_93: - 7400-9300Å
FIBERID:	COMMENTS_PERSON:	
OBJID:	CALIBFLUX:	
	CALIBFLUX_IVAR:	